Universidade de Aveiro Departamento de Química
Ano 2014

Frederico Miguel Horta de Albuquerque de Moura Relvas

Estudo cinético da hidrólise de biomassa sob condições de alta pressão

Kinetic study of biomass hydrolysis under high pressure conditions

Universidade de Aveiro Departamento de Química
Ano 2014

Frederico Miguel Horta de Albuquerque de Moura Relvas

Estudo cinético da hidrólise de biomassa sob condições de alta pressão

Kinetic study of biomass hydrolysis under high pressure conditions

Tese apresentada à Universidade de Aveiro para cumprimento dos requisitos necessários à obtenção do grau de Mestre em Engenharia Química, realizada sob a orientação científica do Doutor Rafał Marcin Bogel-Łukasik, Investigador Auxiliar da Unidade de Bioenergia do Laboratório Nacional de Energia e Geologia de Lisboa e, do Professor Doutor Carlos Manuel Silva, Professor Auxiliar do Departamento de Química da Universidade de Aveiro.

Dedico este trabalho ao meu irmão, tio e avó, amigos e namorada. A todos um muito obrigado pela ajuda, apoio e motivação.

o júri

presidente

Prof. Doutora Maria Inês Purcell de Portugal Branco
Professora Auxiliar da Universidade de Aveiro

Prof. Doutor Armando Jorge Domingues Silvestre
Professor Auxiliar com Agregação da Universidade de Aveiro

Doutor Rafał Marcin Bogel-Łukasik
Investigador Auxiliar da Unidade de Bioenergia do Laboratório Nacional de Energia e Geologia, I. P.

agradecimentos

Gostaria de agradecer a todos os que me ajudaram e apoiaram nesta longa jornada. Um particular obrigado ao Dr. Rafał Łukasik pela fantástica orientação, ajuda e paciência.

À Rita Morais, não só pela sua disponibilidade, acompanhamento e ajuda em todo o trabalho experimental e teórico, mas também por toda a amizade, apoio e preocupação .

Aos meus colegas André Lopes, Cláudia Tavares, Rute Neves, Sofia Graça e Vanessa Carvalho por todos os momentos de boa disposição e entreajuda.

A todas as outras pessoas da Unidade de Bioenergia do LNEG, que também me ajudaram ao longo da minha presença e que sem elas, este trabalho não seria possível.

À Universidade de Aveiro, ao Departamento de Química e aos seus docentes, em especial ao Prof. Doutor Carlos Manuel Silva, Prof. Doutor Francisco Avelino Freitas e Prof. Doutora Inês Portugal, pois foi graças a eles que cheguei até aqui.
A todos os meus colegas de universidade em especial ao Gonçalo Calças, Tiago Bernardo e Catarina Carvalho.

Por fim, um muito obrigado à minha família, irmão, tio e avó, assim como à minha namorada, pois foram eles o grande suporte ao longo desta caminhada.

Um muito obrigado!

palavras-chave

Biomassa, biorrefinaria, pré-tratamento, autohidrólise, hemicelulose, dióxido de carbono, fluídos supercríticos, cinética.

resumo

O presente trabalho focou-se no estudo cinético do pré-tratamento de biomassa lignocelulósica, em particular no processo de autohidrólise assistido com dióxido de carbono. O estudo foi feito fixando a temperatura em 180 ºC, variando a pressão entre 0 (ausência de CO_2), 20, 35 e 50 bar. Para todas as gamas de pressão foram feitos ensaios isotérmicos entre 0 e 45 minutos.

Os pré-tratamentos resultaram em 3 fases, líquida, sólida e gasosa, que foram analisadas por HPLC. A fase líquida é consituída essencialmente por açúcares (monómeros e oligómeros) provenientes maioritariamente do xilana, encontrando-se também ácido acético e produtos de degradação, tais como furfural e ácido fórmico. Por sua vez, as fracções de lignina e celulose na fase sólida aumentaram, sendo mais evidente para tratamentos mais longos. Em relação à fase gasosa, não foram encontrados quaisquer produtos de hidrólise da biomassa.

Com base na literatura e nos resultados experimentais, foram desenvolvidos 4 modelos cinéticos para prever o comportamento da hidrólise da biomassa, correspondentes à fracção de xilana, arabinoxilana, celulose e grupos acetilo.

De acordo com os resultados obtidos, concluiu-se que o uso de CO_2 é útil para fraccionamento selectivo da biomassa, nomeadamente da fracção de hemicelulose e de celulose amorfa, apresentando também melhores resultados do que a autohidrólise na produção de xilooligossacarídeos (XOS), com um máximo de concentração de 14.76 $g \cdot L^{-1}$ para 50 bar vs. 13.62 $g \cdot L^{-1}$ na autohidrólise. Além disso, a conversão de oligomeros em monómeros é proporcional à pressão e favorecida pela presença de CO_2.

Quanto aos modelos cinéticos apresentam uma boa correlação com os dados experimentais, com um R^2 mais alto de 0.9986. No pior caso, o R^2 foi de 0.7865 que, tratando-se de uma reacção complexa, pode ser considerado um boa resultado. Apesar das constantes cinéticas mostrarem um aumento da hidrólise de xilana e arabinana na presença de CO_2, estas decrescem em pressões mais elevadas.

Por sua vez, os grupos acetilo também mostram resultados bastante consistentes, com o R^2 mais baixo de 0.9491. A remoção de ácido acético parece ser prejudicada pela presença de CO_2, enquanto os resultados da hidrólise de glucano sugerem uma cinética de ordem zero, uma vez que a concentração dos produtos aparenta ser independente da concentração dos diferentes produtos.

keywords

Biomass, biorefinery, pretreatment, autohydrolysis, hemicellulose, carbon dioxide, supercritical fluids, kinetics.

abstract

This study was focused on the kinetics of lignocellulosic biomass pre-treatment, in particular CO_2-assisted autohydrolysis. The temperature was fixed at 180 ºC, varying pressure from 0 (CO_2-free autohydrolysis), 20, 35 to 50 bar. For every pressure, a set of isothermal reactions was performed for various reaction times from 0 and 45 minutes.

The pre-treatment resulted in a liquid, solid and gas phases, which were analyzed by HPLC. The liquid phase is essentially composed by sugars both in oligomer and monomer forms, mainly from xylan, also containing acetic acid and degradation products such as furfural and formic acid. In turn, there was an improvement of lignin and glucan's fraction in the solid residue, being more pronounced for longer treatments. Regarding gas phase collected during depressurization, no traces of products from biomass hydrolysis were found.

Basing on the literature and experimental results, 4 kinetic models were developed to predict the behavior of the biomass hydrolysis. Models for xylan, arabinoxylan, glucan and another for acetyl groups were presented.

According to the results, the use of CO_2 is beneficial for the selective fractionation of biomass, including hemicellulose and amorphous cellulose fractions. Beside, CO_2 favors the production of xylooligosaccharides (XOS) achieving a maximum concentration of 14.76 $g \cdot L^{-1}$ at 50 bar assay vs 13.62 $g \cdot L^{-1}$ in case of autohydrolysis. Furthermore the conversion of oligomers to monomers is directly proportional to pressure and is enhanced by CO_2 presence.

With respect to the developed kinetic models, all showed good correlation with experimental data, with R^2 as high as 0.9986. In the worst case, the R^2 was 0.7865 what considering the so complex multistep analysis process can be acknowledge as a good result. Despite kinetic constants showed an increase of hydrolysis rate of xylan and arabinan in the presence of CO_2, they decreases for higher pressures used.

In turn, the model for acetyl groups also shows very consistent results with the lowest R^2 of 0.9491. The removal of acetyl groups seems to be impaired by the carbon dioxide presence. With respect to glucan, the obtained data shows that reactions are close to zero order as they are independent on the products' concentrations.

List of Contents

List of Figures

List of Tables

Nomenclature

a	Peng-Robinson adjustable parameter
AcO	Acetyl groups
AcOH	Acetic acid
ArXn	Arabinoxylan
AOS	Arabinooligosaccharides
AX	Arabinoxylose
AXOS	Arabinoxyloolygoscacharides
b	Peng-Robinson adjustable parameter
CSP	Combined severity factor
DP	Degradation products
F	Furfural
FTIR	Fourier transform infrared spectorscopy
GHG	Greenhouse gas
Glc	Glucose
Gn	Glucan
GOS	Glucoligosaccharides
HMF	Hydroxymethylfurfural
HPLC	High performance liquid chromatography
k, l, m	Reaction rate constant
k	Henry constant
Log R_0	Severity factor
LOI	Lateral order index
M	Molarity
R	Gas constant
R^2	Correlation coefficient
RPM	Rotations per minute
ScF	Supercritical fluid
UV/VIS	Ultraviolet/Visible
w	Weight
x	Fraction
XOS	Xylooligosaccharides

Greek Letters

α	Susceptible Fraction
β	Remaining Soluble Fraction in the Solid
ρ	Density
Ø	Diameter
σ	Reaction rate order
τ	Reaction rate order
φ	Reaction rate order
ω	Ascentric factor

	Subscript
0	At time zero
c	Critical
h	Henry
H	High molecular weight
L	Low molecular weight
r	Reduced
tmax	Maximal time studied
w	Weight

The work presented in this thesis was presented in various forms as listed below:

Peer-reviewed papers

F. M. Relvas, A. R. C. Morais, R. Bogel-Lukasik, The kinetics study of CO_2-assisted biomass hydrolysis, J. Supercritical Fluids, 2014, submitted.

F. M. Relvas, A. R. C. Morais, R. Bogel-Lukasik, The biomass fractionation in high pressure systems with CO_2, Bioresource Technology, 2014, submitted

Oral communications

F.Relvas, M. Brenner, A. da Costa Lopes, V. Carvalho, A. R. C. Morais, S. P. Magalhães Silva, A. Mata, L. B. Roseiro, R. Bogel-Lukasik, Biorefinery concept with green solvents towards the phenolic valorization, 8th World Congress on Polyphenols Applications, VI.2014, Lisbon, Portugal.

V. Carvalho, F. M. Relvas, A. da Costa Lopes, A. R. C. Morais, S. P. Magalhães Silva, A. Mata, L. B. Roseiro, R. Bogel-Lukasik, Green chemistry and biorefineries – common future?, Lignocellulosic Crops as feedstock for Future Biorefineries, Summer Course of FIBRA Project,VII.2014, Caparica, Portugal.

Poster presentation

A. R. C. Morais, A. M. da Costa Lopes, F. M. Relvas, A. C. Mata, L. B. Roseiro, R. Bogel-Lukasik, The application of green technologies in production and extraction of phenolic compounds from industrial residues in the frame of the biorefinery concept, 8th World Congress on Polyphenols Applications, VI.2014, Lisbon, Portugal.

This work was supported by the Fundação para a Ciência e a Tecnologia (FCT, Portugal) through Bilateral Cooperation project FCT/CAPES 2014/2015 (FCT/1909/27/2/2014/S). The work was also supported by CAPES (Brazil) though the Pesquisador Visitante Especial 155/2012.

1. Introduction

Although fossil fuels have been playing an important role in our society providing high quality living standards, they also generated several environmental problems being responsible for air pollution and global warming, caused mainly by the Greenhouse Gas (GHG) emissions [1]. Apart from environmental concerns, it is also known that fossil fuels' feedstock availability will become an issue in mid or long-term, originating in its deficiency as well as geo-political and economic concerns due to its heterogeneous worldwide distribution. Consequently, there is a need to find alternative raw feedstocks and processes in order to create a sustainable way of future human existence [1]. However, despite the emergence of many alternative energy sources, none of these is fully capable to substitute fossil fuels' demands. For example, nowadays a 80% of the primary energy consumption derives from fossil fuels, among which 58% share is dedicated to transport sector [2]. That is why the main force is put on the transition from fossil to renewable feedstock in the fuel production. Consequently, many countries have adopted different measures to introduce biofuels such as those addressed by Environmental Protection Agency (EPA) in US and Directive 2009/28/EC in European Union [3-5].

Non-energy applications represent only about 9% of all fossil fuels and 16% of oil products [6-9]. These relatively low percentages, means in fact, a significant release of CO_2 to the atmosphere related to the production of diverse chemicals. From the technical point of view, almost all of commodities produced from fossil fuels could be substituted by bio-based products, but the production costs are often still non-competitive comparing to current low price of petrochemical origin products [9]. According to the US Department of Energy, a lot of these commodities for example levulinic and glucaric acid, glycerol, sorbitol, xylitol, etc. can be successfully produced from biomass, and later converted to a variety of value added bio-based chemicals or materials [10]. From this perspective, a bigger relevance should be given to bioproducts, but aforementioned obstacles hinder the potential of these products [8]. Fortunately, a greater effort is being done in the recent years to change this paradigm and new concepts of "*biorefinery*"[11] and significant increase of "green chemistry"[12] role have emerged.

1.1. Biorefinery and the role of Green Chemistry

The idea to produce bio-based commodities is not new. Since the beginning of the last century (and even earlier) chemists and engineers developed processes to make a large diversity of products, including those obtained from waste. One of them was Hale and Herty who in 1925 founded "Chemurgy" and their policy was the use of agricultural waste. However, due to dramatically low prices of crude oil, "Chemurgy" went into decline. Nevertheless, a lot of processes and philosophies keep on and, in 1941, a car whose interior was totally made by bio-products was introduced by Henry Ford, whose alternative fuel was pyrolysis of methanol produced from cannabis [4].

Nowadays, biorefinery concept is focused not only on the processing of biofeedstock but also on doing it in a sustainable manner, as was stated in the 1st International Green Biorefinery Conference: "biorefineries represent complex (to fully integrated) systems of sustainable, environmentally and resource-friendly technologies for the comprehensive (holistic) material and energetic utilization as well as exploitation of biological raw materials in form of green and residue biomass from a targeted sustainable regional land utilization" [13]. Thus, during chemical's production energy demands, hazardous chemical use and production should be avoided. In these terms, the integration of green chemistry into biorefineries is mandatory, reducing the energy demands, decreasing hazardous chemical use and production as well as adding value to the sustainable use of the biomass [14]. The green chemistry concept is based on the twelve principle compiled by Anastas and Warner [12] (Figure 1.1). Putting it into practice, numerous chemicals might be produced in future biorefineries with low residue footprint [15]. Nonetheless a lot of research is still needed.

Figure 1.1 – The twelve principles of Green Chemistry [12].

Currently, since large amounts of biofuels are necessary to meet the policy regulations and 1st and 2nd generation biofuels are commercially uncompetitive, thus the development of biorefineries is a need [16]. In terms of operations, biorefinery's approach is similar to petrochemistry, where a separation into main streams is firstly done, which being subsequently processed lead to a wide range of products. In order to maximize their potential, bio and fossil refineries have a well-defined system in family trees, producing either basic chemicals or sophisticated products [4]. Figure 1.2 shows a schematic presentation of biorefinery concept.

The main issue to be resolved is the question about the potential of future biorefineries to have a significant impact in the reduction of non-renewable sources consumption. According to Perlack et al. [17], biomass feedstock has a potential enough to reduce more than one-third of the transportation fuel demand in United States and it is expected that by 2020 about 25% of industrial feedstock chemicals (compared to 1995) will be supplied from bio-based industry [1]. In addition, all contributions must be considered in order to reduce fossil dependence, but novel technologies still being in the

infancy and capital investment needed to rearrange the today's production of goods and services and to make bio-products profitable and competitive must to be taken in account as well. Accordingly, biorefineries' development represents an important step for the future of energy, fuels and chemical products in a sustainable way [17].

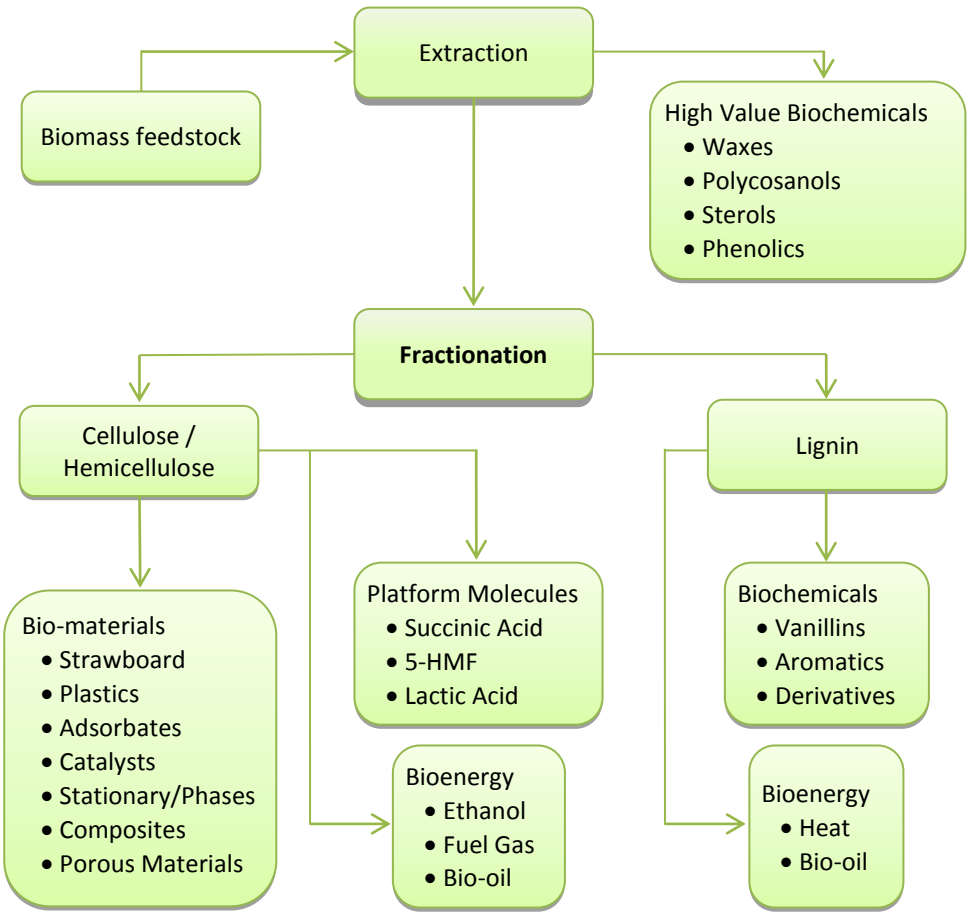

Figure 1.2 – Lignocellulosic feedstock biorefinery (adapted from Kamm et al. [4]).

1.1.1. The biorefineries feedstock

Biorefineries purpose to a sustainable production of goods and services [11]. For this reason, all the feedstock must derive from renewable sources, such as agricultural wastes, forest residues, dedicated crops, etc. Nevertheless, the use of some of these feedstocks may induce divert issues that must be addressed. For example, direct and indirect alterations of land use may disturb the natural equilibrium of carbon cycle. Moreover, in the case of 1st generation biofuels, the competition for the same feedstock by fuel and food sectors is accused to contribute to higher food prices [18]. Accordingly, a lot of considerations should be kept in mind to guarantee a sustainable transition to

renewable feedstocks, contradicting what have been done in the recent years in case of biofuel's production.

Biomass and especially diverse types of lignocellulosic raw materials are nowadays one of the most important energy sources, having an estimated annual production of 10-50 billion metric tons [18, 19]. Figure 1.3 depicts the structure of the lignocellulosic material. Lignocellulosic material is composed by three main fractions: cellulose and hemicellulose, which are constituted by chains of sugar molecules representing a 35-50% and 20-40% of biomass composition, respectively. The third main fraction is lignin composed by a complex polymer of aromatic alcohols (10-25% of biomass dry-weight), depending on the source, geographic location, climacteric conditions, etc. [19, 20].

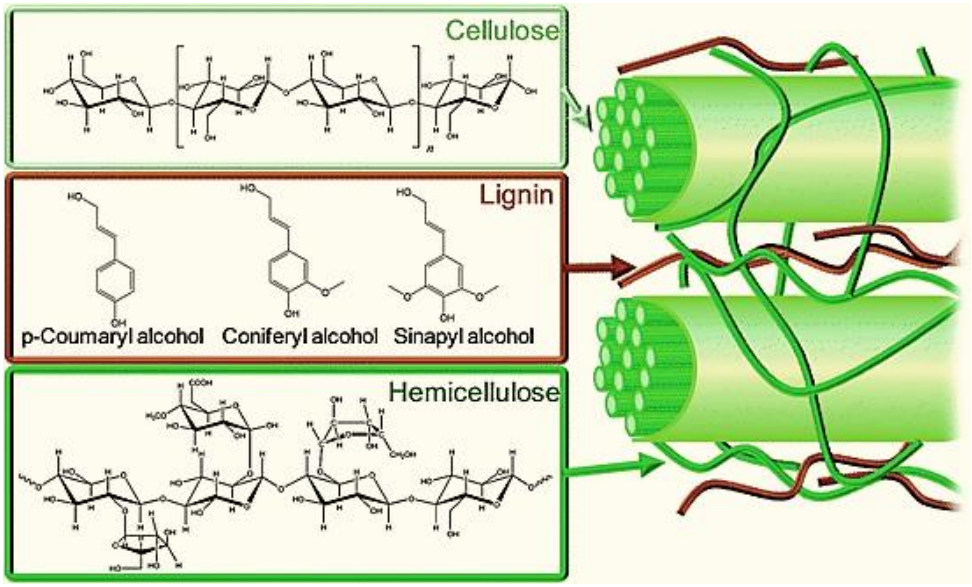

Figure 1.3 – Lignocellulosic materials' structure (Adapted from Alonso et al. [21]).

Cellulose is the main constituent of the plant cell walls, having a partially crystalline structure composed by glucose monomers liked by β-1,4 glycosidic bonds, which can be hydrolyzed to glucose by *cellulases*, and further fermented to produce ethanol [22] or converted by biological or chemical ways to other value added products.

Hemicellulose is the connecting material between cellulose and lignin in cell walls. Unlike cellulose, it has a non-crystalline structure that consists of a branched heteropolymers with a low degree of polymerization (around 200), predominantly xylan in agricultural biomass, while softwood mainly contain glucomannan. In addition to the backbone, hemicellulose also may contain arabinose, glucuronic acid and other molecules

[22, 23]. The predominant part of hemicellulose research is focused on xylan conversion, which comprises between 8 and 25% of the entire biomass composition [21].

The third major fraction of lignocellulosic biomass is lignin. Lignin monomer structure is based on three phenylpropanoid monomer, *p*-coumaryl alcohol (4-hydroxyl phenyl, H structure), coniferyl alcohol (guaiacyl, G structure) and sinapyl alcohol (syringyl, S structure). Being rigid, impermeable and resistant against microbial attack and oxidative stress, lignin offers cellulose protection against microbial and enzymatic degradation [23].

According to the data collected by Kim and Dale [46],wheat straw used in this study, as well as other crop residues like rice straw, corn stover and sugar cane bagasse, is one of the most favorable feedstocks for energy production (e.g bioethanol) worldwide. Wasted crops have a potential to produce about 49.1 GL of bioethanol per year, coming from the 7.39×10^{9} tons produced yearly. Summing this with the lignocellulosic biomass potential, the bioethanol production could substitute about 32% of the global gasoline consumption (around 353 GL). Moreover, residues obtained from ethanol production have a potential to generate 458 TWh of electricity, corresponding to 3.6% of the world electricity production [24]. Nevertheless, it is obvious that biomass availability is neither homogeneous nor similar in type of biomass feedstock. Thus, biorefineries should be done according to the local market, land and feedstock readiness, etc. Table 1.1 demonstrates the potential available area and biomass type for bioethanol production.

In order to guarantee sustainability of future biorefineries, it is important to consider only the wastes as feedstock, avoiding competition between other sectors especially food industry for the same feedstock [24]. Accordingly, other sources should be considered when necessary, requiring a high versatility of technologies used in future biorefineries.

Table 1.1 – Wasted crop and lignocellulosic biomass potential for bioethanol (adapted from Kim and Dale [24]).

	Africa	Asia	Europe	North America	Central America	Oceania	South America	Subtotal
Wasted crop (10^6 metric ton)								
Corn	3.12	9.82	1.57	0.30	1.74	0.01	4.13	20.7
Barley	0.17	1.23	2.01	0.01	0.01	0.19	0.04	3.7
Oat	0.01	0.06	0.43	0.01	0.00	0.001	0.05	0.6
Rice	1.08	21.86	0.02	0.96	0.08	0.02	1.41	25.4
Wheat	0.83	10.28	4.09	0.02	0.24	0.82	0.91	17.2
Sorghum	2.27	0.54	0.01	0.00	0.13	0.00	0.18	3.1
Sugar cane	0.46	1.64	0.00	0.00	0.36	0.00	0.74	3.2
Subtotal	7.94	45.43	8.13	1.30	2.56	1.05	7.45	73.9
Lignocellulosic biomass (10^6 metric ton)								
Corn stover	0.00	33.90	28.61	133.66	0.00	0.24	7.20	203.6
Barley straw	0.00	1.97	44.24	9.85	0.16	1.93	0.29	58.4
Oat straw	0.00	0.27	6.83	2.80	0.03	0.47	0.21	10.6
Rice straw	20.93	667.59	3.92	10.95	2.77	1.68	23.51	731.3
Wheat straw	5.34	145.20	132.59	50.05	2.79	8.57	9.80	354.4
Sorghum straw	0.00	0.00	0.35	6.97	1.16	0.32	1.52	10.3
Bagasse	11.73	74.88	0.01	4.62	19.23	6.49	63.77	180.7
Subtotal	38.00	923.82	216.56	218.90	26.14	19.70	106.30	1549.4

1.1.2. Biorefineries products

Nowadays biorefineries are very often associated to biofuels' production. However, as mentioned by the Department of Energy of U.S in the Annual Energy Outlook 2007 "The value of co-products will play a significant role in determining which crops are most profitable for farmers to grow, and biofuels producers to use", thus the profit of biorefineries might be dependent of co-products once they are often more valuable than fuels produced [25]. Besides, co-product usage also reduces wastes enhancing the process sustainability.

Apart from ethanol, cellulose might be the source of some chemicals such as 5-hydroxymethylfurfural (HMF) showing a great potential of cellulose alternative valorization, once HMF can be used as a building block for the production of other chemicals using green technologies [26]. Furthermore, hemicellulose hydrolysis allows

producing a great variety of goods too. Some examples include xylooligosaccharides (XOS) with applications in pharmaceutical industries and furfural, which can be used as decolorizing agent, reactive solvent, feedstock for other furan derivatives' production, etc. [27, 28]. In the case of XOS, they exhibits prebiotic activities, and because of this, they found an application in food and pharmaceutical industries [28, 29]. Lignin, despite being usually associated to low value applications (predominantly lignosulfonates), recent research showed that this fraction have a wide range of applications namely in polymer industries. However, the isolation of lignin from wood still challenging and requires extensive research [30, 31].

1.2. Biomass pre-treatments

Lignocellulosic materials have a very rigid composition, which make them unlikely for direct hydrolysis process. In addition, because cellulose has a crystalline structure, its enzymatic digestibility is very low, even more in rigid and complex matrix of lignocellulose composite [32]. For that reasons, a biomass pre-treatment plays an important step in the valorization process in biorefineries leading to the increase of the glucan and xylan accessibility to enzymatic attack.

Depending on the pre-treatment approach used, the methods of fractionation can be classified into four categories: physical, chemical, physico-chemical and biological. Each pre-treatment leads to a specific output with cons and pros typical for each process. In general, physical treatments have lower performances associated to higher costs. In its turn, chemical treatments show higher selectivities [33] and among this type of pre-treatments are: acid hydrolysis, which usually uses concentrated or diluted sulfuric acid and achieves high sugar yields; alkaline treatments, where cellulose digestibility is increased by separation of lignin linkages [34-36]. The disadvantage of chemical pre-treatment is the requirements of harsh reaction conditions representing negative impacts on the process (e.g. corrosion). For this reason, the physico-chemical pre-treatments are commonly used, once they allow to process biomass under milder conditions and to achieve higher yields of the desired products, despite slightly higher cost due to the elevated pressures and temperatures. Finally, although biological pre-treatments are not been well developed, they seem to have a big potential, once the operating conditions

are much less demanding regarding to energy and chemicals uses [33], however the low yield is still a significant challenge.

An efficient fractionation of different biomass fractions is commonly intended. In addition hemicellulose, cellulose and lignin hydrolyses are also desired, once their hydrolysates are the feedstock for diverse chemicals' production [37]. Because none of the pre-treatment methods provide high yields of all desired products simultaneously, they are often combined. Thus, the selection of the process must be done according to the desired outcome and the physical and chemical characteristics of biomass type used.

In the recent years, the use of alternative solvents such as ionic liquids (IL) and sub- or supercritical fluids (ScF) (e.g. CO_2) have been explored intensively, aiming at making the process "greener" by reducing the process severity in terms of energy and time consumption as well as avoiding the use of non-environmentally friendly chemicals [38-40].

1.3. CO_2 and Supercritical Fluids

The interest in carbon dioxide use as reagent and/or solvent has been increasing in more than last 20 years. Being non-flammable, CO_2 has a significant advantage in comparison to many other classical chemicals. In addition, CO_2 is highly abundant in waste gases and it can be captured and separated in many processes [41, 42].

CO_2 has interesting characteristics above its supercritical conditions particularly due to its moderated critical parameters (31 ^{o}C and 72.8 bar). A supercritical fluid is a substance above its critical temperature and pressure, T_c and P_c respectively and below the condensation conditions[43]. The Figure 1.4 shows the supercritical fluid (e.g. CO_2) phase diagram, which explains the variation of its physical state as function of the temperature and pressure.

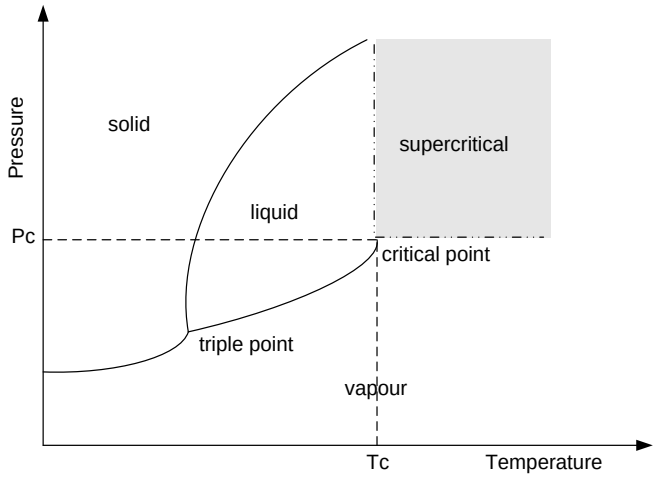

Figure 1.4 – Phase diagram for a supercritical fluid. The critical point is the point at which the densities of the liquid and gas become identical and the fluid is said to be supercritical. Note that in this diagram the pressure scale is nonlinear.

Raising both temperature and pressure along the boiling curve, CO_2 density will decrease in the liquid phase due to its thermal expansion, while the reverse happens in the gas phase [44]. As it can be seen in Figure 1.5, the liquid and gas phases are no longer distinguishable when supercritical state is reached (image on the right side). Regarding pressure dependence, density sharply increases with pressure near compressible region, while at higher pressures it happens more gradually. Because of large compressibility, density's fluctuations occur, leading to areas with high and low densities, which will affect solvent power and this serve as basis for the technical use of supercritical fluids [43].

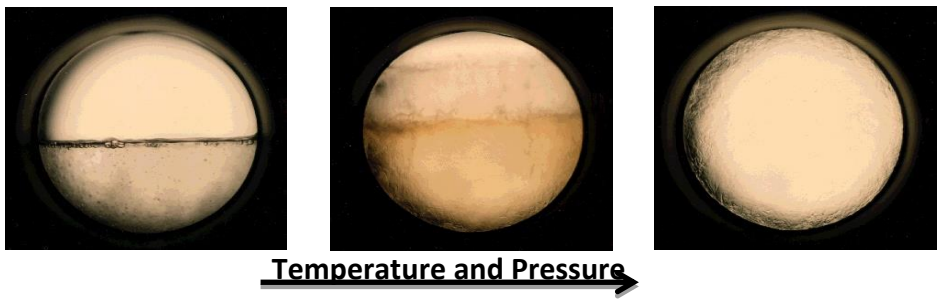

Figure 1.5 – Visual evolution of supercritical fluid towards the boiling curve (adapted from [44]).

According to the characteristics stated before, ScF can be described as an intermediate between liquid and gas sharing the advantages of both, such as high diffusivity and low viscosity and density, which can be observed in the Table 1.2 for CO_2 particular case [1].

Table 1.2 – Physical properties of CO_2 as gas, liquid and ScF (adapted from [45]).

Property	**Gas**	**Liquid**	**ScF**
Diffusivity ($cm^2 \cdot s^{-1}$)	10^{-1}	10^{-5}-10^{-6}	10^{-3}
Viscosity ($Pa \cdot s$)	10^{-5}	10^{-3}	10^{-4}
Density ($g \cdot cm^{-3}$)	10^{-3}	1	(1-9)x10^{-1}

In the case of CO_2, a lower surface tension might be observed in comparison to conventional organic solvents, leading to a higher diffusivity and consequently to a better penetration in complex geometries [41]. Besides, due to its easily achievable supercritical conditions, design equipment for $scCO_2$ usage is much simple than for other fluids e.g. water. Moreover, its separation from solution is very easy at atmospheric pressure as it loses the solvent power being completely insoluble in the product mixture and vice versa [46, 47].

1.4. CO_2-assisted autohydrolysis

Autohydrolysis is a hydrothermal process used in biomass pre-treatment in order to hydrolyze hemicellulose, resulting in a liquor rich in XOS, acetic acid, xylose and its degradation's products. It comprises hot water at temperatures between 150 and 230 °C and pressure above the saturation point. The hydrolysis of hemicellulose can be illustrated according to the Equation 1.1 [48].

$$\text{Hemicellulose} \rightarrow \text{Xylan} \rightarrow \text{XOS} + \text{acetic acid} \rightarrow \text{Xyl} \rightarrow \text{furfural} \rightarrow \text{formic acid}^{1} \quad \text{Eq.1.1}$$

The temperature range represents an important factor because under 100 °C there is no effect of hot water on biomass [34, 49], whereas above 220 °C the cellulose hydrolysis becomes more noticeable [50-52]. The quantity of different products is also strongly dependent on the biomass residence time [53].

The formation of the hydronium ion (H_3O^+) from the water autoionization catalyzes the first stage of the reaction, leading to the depolymerization of hemicellulose due to the glycosidic linkage rupture. Subsequently, resulting acetic acid enhances the hydrolysis, forming more XOS and subsequent products [38]. The described autohydrolysis works similarly to acid hydrolysis, but the avoidance of neutralization

[1] Depending on the type of biomass, different types of oligosaccharides (and consequently monosaccharides) might be formed.

need, low equipment corrosion risk and lower by-product formations are advantages in case of autohydrolysis [54].

The pre-treatment permits to obtain a solid residue rich in cellulose and lignin and a liquor rich in XOS and resulting products [55]. At the same time, residues of HMF and levulinic acid (from HMF deterioration) may also be present in the liquid phase, resulting from amorphous cellulose hydrolysis [56]. The solid phase can be recovered for processing for the production of bioethanol and some platform chemicals namely HMF and levulinic and formic acids [57]. The liquor composition is strongly affected by the pre-treatment conditions [19, 29, 38, 54, 58]. Thus, for comparison purposes [49, 59] a severity factor ($logR_0$) defined by Overend and Chornet is usually used to measure the effects of time and temperature according to Equation 1.2, where t is time expressed in minutes, T relates to temperature in °C, 100 is the base temperature (100 °C) and 14.75 is an empirical constant.

$$\mathrm{R_0} = \int_0^{\mathrm{t}} \mathrm{e}^{\frac{\mathrm{T(t)-100}}{14.75}}\,\mathrm{dt} \qquad \text{Eq.1.2}$$

Recent studies [38, 58, 60, 61] using pressurized water in the presence of CO_2 showed an improvement of the efficiency of biomass processing in comparison to those for only water treatments. A possible explanation might be owing to the *in-situ* carbonic acid formation, making the water more acidic and by this enhancing the hemicellulose dissolution and retaining cellulose and lignin in solid phase [62]. One of the most important aspects in this complex CO_2-H_2O system is the solubility of CO_2 in water. The solubility of CO_2 is water mostly dependent on temperature and pressure of CO_2. Regarding temperature dependence, solubility of CO_2 decreases with an increase of temperature [63]. In turn, when pressure increases, solubility also increases [63]. Thus, the carbonic acid formation (Equation 1.3) in water-CO_2 system is favored at lower temperatures and increases with the CO_2 pressure [64]. This may consist of an improvement in processes benefited by acidity (chemical effect of CO_2).

$$\mathrm{CO_2 + 2H_2O \rightleftharpoons H_3O^+ + HCO_3^-;\ HCO_3^- + H_2O \rightleftharpoons CO_3^{2-} + H_3O^+} \qquad \text{Eq.1.3}$$

Despite being a week acid, carbonic acid does not require a further neutralization and is less corrosive for environment than stronger acids (at the same concentration), consisting of an advantage when comparing to other acids like H_2SO_4. Moreover, the

presence of CO_2 increases the pressure, which reduces the evaporation rate of water and as a result, processes where water acts as a reactant are enhanced by the pressure effect of the CO_2 presence. Accordingly, the behavior of CO_2-water system is an important guide to select the best operation conditions during experiments.

Due to the described effect of CO_2, the classical severity factor is less accurate [61]. Thus, van Walsum [65] based on the combined severity factor proposed by Chum et al. [66] shown is Equation 1.4. proposed the approximation of pH by a function of partial pressure of CO_2 as demonstrated in Equation 1.5 [65].

$$\mathrm{CS}_{\mathrm{P}_{\mathrm{CO}_2}} = \log(\mathrm{R}_0) - \mathrm{pH} \qquad \text{Eq.1.4}$$

$$\mathrm{pH} = 8.00 \times 10^{-6} \times \mathrm{T}^2 + 0.00209 \times \mathrm{T} - 0.216 \times \ln\left(\mathrm{P}_{\mathrm{CO}_2}\right) + 3.92 \qquad \text{Eq.1.5}$$

2. Objectives

The objective of this work was to study the effect of high pressure CO_2-H_2O technology on the deconstruction of the lignocellulosic structure of wheat straw with the kinetics study of the occurred reactions. The kinetics study of hemicellulose and cellulose fractions allowed to understand the effect of the examined conditions on the reactions.

3. Materials and methods

3.1. Feedstock and reagents

Wheat straw supplied by Estação Nacional de Melhoramento de Plantas (Elvas, Portugal) was used as feedstock. The milling of the raw material was done using a knife mill Warring, Snijders Scientific, Netherlands, in order to obtain particles smaller than 1.5 mm, while the processed solids were milled using a knife mill IKA® WERKE, MF 10 basic, Germany, to get <0.5 mm particles. The moisture content determination of the raw material and the processed solids (before and after milling) was done by over-drying at 100 ^{o}C.

The biomass used in the experiments presented in this work was from the same lot as the work already presented in literature [38] thus, the composition taken from literature is depicted in Table 2.1.

Table 2.1 - Composition of wheat straw used as feedstock (% by dry weight)[38].

Component	**Composition (wt.%)**
Cellulose[1]	38.6 ± 0.1
Hemicellulose	24.9
• Xylan	19.2 ± 0.6
• Arabinan	3.0 ± 0.1
• Acetyl Groups	2.7 ± 0.2
Klason Lignin	17.7 ± 0.1
Protein	4.7 ± 0.1
Ash	10.7 ± 0.1
Others	3.5 ± 0.1

Distilled water (18.2 MΩ·cm^{-1}) produced by Purelab Classic Elga system together with CO_2 with 99.99% purity commercialized by Air Liquide, AlphaGaz™ gamma, Paris, France were used in the high-pressure pre-treatment processes. An ethanol solution (96% v·v^{-1}) acquired from Carlo Erba Group, Arese, Italy, was used to recover the gas phase during depressurization.

For the chemical analysis, an aqueous sulfuric acid solution 72% (w·w^{-1}) was prepared using a 96% (v·v^{-1}) solution commercialized by Panrec Química, Barcelona,

[1] Measured as glucan.

Spain. The same quality of distilled water as previously mentioned was used for processed solids washing and chemical characterization of the liquor and solid phases.

All FTIR samples were prepare with >99.5 purity KBr from Sigma-Aldrich Co. (St. Louis, MO, USA).

3.2. Pretreatment Procedure

3.2.1. Reaction

Mixture of 7.5 g of biomass dry weight and 75 g of distilled water were prepared and transferred to a 160 mL stainless steel high-pressure Parr 4655 reactor (Parr Instruments Company, Moline, Illinois, USA) coupled with the control unit Parr 4842 used to control the temperature, pressure and agitation of the reaction mixture. Next, reactor was properly closed and in case of reactions with CO_2, was pressurized at room temperature until reaching the desired initial CO_2 pressure. For this purpose CO_2 with an initial temperature of -9 ^oC was used and 17 ^oC in the reaction, which permitted to minimize the CO_2 density variations due to the temperature changes. The experiments started when pressure stabilizes at the required level and the reaction mixture was started to be stirred (75 rpm) and heated. Time, temperature and pressure data were collected regularly. For the kinetics purposes different reaction time were examined at settled isothermal conditions (180 ^oC) and initial pressures of 0 (autohydrolysis), 20, 35 and 50 bar.

When the required reaction time ran out, the heating was turned off and the reactor was cooled down rapidly using ice and water to quench the occurring reaction. Once the internal temperature was as low as the initial temperature, the reactor was slowly depressurized and the gas phase was collected to a flask containing a known amount (around 5 g) of ethanol.

3.2.2. Chemical analysis

3.2.2.1. Solid's moisture and liquors dry weight's determination

To measure the moisture content of the solid (treated and non-treated) the samples were milled to a particle size <0.5 mm. For each solid and liquid samples, two nickel plates were placed in a stove at 100 ^oC for at least 18 h, being further weighed to

obtain the tare weight (before weighing, the plates were placed in a desiccator for approximately 30 minutes). 1 g of solid samples were weighed into the plates and placed in the same oven. After 18 h their dry weight were registered. In the case of solid samples used for quantitative acid hydrolysis, 0.3 g was weighed while for liquors 2 g for each sample was used. All the measures were made using the analytical balance.

3.2.2.2. Characterization of produced solid

The solid phase produced during pre-treatment was washed using 150 mL of distillated water (twice the volume used in the reaction) in order to remove hydrolysate remaining in the solid phase. Such formed solid phase was analyzed after treatment with a 72% ($w \cdot w^{-1}$) H_2SO_4 according to the standard methods [67]. In particular, 0.1999 - 0.2010 g of the sample were transferred to a test tube, adding 2 mL of the H_2SO_4 solution. The tubes were placed in a water bath at 30 ^oC for 1 h. During the first 30 min, the tube's content was stirred every 10 minutes for 10 seconds. After 1 h, the solutions were transferred to previously weighed 250 mL glass flasks. The tubes were then washed using distilled water and washing water was transferred to the same flasks until 59.024 g was reached allowing to get a 4% H_2SO_4 solution. Subsequently, the flasks were autoclaved (Uniclave, Portugal) for 1 h at 121 ^oC. The flasks were weighed before and after autoclaving. Resulting solutions were filtered using previously dried crucibles with number 3 porous plate. A liquid sample was collected from every flask using a syringe filter (0.22 μm) for HPLC analysis Agilent 1100 series HPLC system, Santa Clara, CA, USA, equipped with refractive index detector and a Biorad Aminex HPX-87H column (Hercules, CA, USA) at 50 ^oC with a flow rate of 0.4 $mL \cdot min^{-1}$ of a 5 mM H_2SO_4 solution, which allowed the quantification of monosaccharides and acids. The previously mentioned crucibles were placed in the oven at 100 ^oC for at least 18 h. Afterwards, they were placed in a muffle furnace Heraeus D-6450, Germany at 550 ^oC for 5 hours. They were later cooled down in a dessicator during 1.5 h. The obtained residue (ashes) was weighed using an analytical balance. The difference between the weights after and before furnace was considered as Klason lignin.

3.2.2.3. Post-hydrolysis of liquor

The produced liquor was obtained by two steps vacuum filtration. In the first step, the filtration was done using quick filtration filters (Ø=150 mm, nº 1235) from Filter-Lab, Microchip Technology Inc., Arizona, USA. A second separation was done with (Ø=150 mm, nº 1242) filters. The pH of the produced liquor was measured using Crison pH-meter.
A liquor sample was filtered using 0.45 µm pore size filters and analyzed using HPLC with a flow rate of 0.6 $mL \cdot min^{-1}$ of a 5 mM H_2SO_4 solution.

As mentioned before, the resultant liquor from the pretreatment contains sugars in both oligomer and monomer forms. Thus to analyze the oligomers' concentration, a post hydrolysis was performed. This treatment consists of the hydrolysis of produced liquid using a 4% H_2SO_4/liquor solution, where all oligosaccharides are hydrolyzed to sugar monomers. Firstly, 1 g of H_2SO_4 aqueous solution (72%) was weighed to a Schott bottle (Schott Duran, Germany) and a 17.225 g of liquor sample was added, obtaining a 4% H_2SO_4 solution, being then autoclaved for 1h at 121 ^oC. The resulting solutions were then filtered using 0.22 µm pore filters from Whatman, GE Healthcare Life Generations, Buckinghamshire, United Kingdom, and were further analyzed by HPLC analogously to the method mentioned above. Furfural and 5-hydroxymethylfurfural (HMF) were detected by an UV/Vis detector at 280 nm. XOS quantification was done by comparison with the liquor results by the difference of xylose concentration after and before post-hydrolysis.

To study the presence of phenolics, the samples were also analyzed by capillary electrophoresis using an Agilent CE G1600AX (Waldbronn, Germany) equipped with a diode array detector (UV-DAD) and using an uncoated fused silica extended light-path capillary. A constant temperature of 30 ^oC was kept in the capillary being firstly conditioned by rinsing sequentially 1 M sodium hydroxide, 0.1 M sodium hydroxide and Milli-Q water, for 20 minutes for each sample. Electropherograms were recorded at 200, 280, 320 and 375 nm and the compounds were identified by comparison with authentic phenolic standards. The remaining solids were placed in an oven at 80 ^oC for at least 48 h and being further stored at room temperature for at least 48 h for further characterization.

3.2.2.4. The FTIR analysis of the formed solids

The FTIR technique, which allows to measure indirectly the cellulose crystallinity [6, 68], was used for solid samples produced during the pre-treatments. For this work about 1.0 mg of sample was milled together with 50 mg of KBr during 10 minutes with the goal of reaching a homogeneous appearance. Then the mixture was pressed with 8.5 tonnes for 5 minutes. The same procedure was made for all examined samples. For analysis of produced samples spectrometer Spectrum BX, Perkin Elmer, Inc. (San Jose, CA, USA), equipped with a DTGS detector and KBr beam splitter, using Spectrum software (Version 5.3.1, Perkin Elmer, Inc.,San Jose, CA, USA) was engaged. The data was acquired by FTIR spectra at 4000-400 cm^{-1} with a resolution of 4 cm^{-1}. For each analysis, the spectrum of the air background was subtracted.

3.2.2.5. Gas phase analysis

The depressurized gas phase was analysed by HPLC with an UV/Vis detector at 280 nm to examine the presence of volatile degradation compounds, namely furfural and acetic acid.

3.2.2.6. Combined severity factor

For the comparison purposes the aforementioned combined severity factor was used. To calculate the combined severity factor the Equations 1.4 and 1.5 were used. In order to study the effect of CO_2 concentration in severity conditions, CO_2 solubility was calculated through Peng-Robinson equation of state [69] and MKP mixing rule using the initial CO_2 pressure and temperature for each pre-treatment:

$$p = \frac{RT\rho}{(1-b\rho)} - \frac{a\rho^2}{1+2b\rho-b^2\rho^2}, \quad \text{Eq. 2.1}$$

$$a = a_c\gamma \quad \text{Eq. 2.2}$$

$$a_c = 0.45723553\frac{R^2T_c^2}{p_c} \quad \text{Eq. 2.3}$$

$$\gamma = [1+\kappa(1-\sqrt{T_r}]^2 \quad \text{Eq. 2.4}$$

$$\kappa = 0.37464 + 1.54226\omega - 0.26993\omega^2 \quad \text{Eq. 2.5}$$

$$T_r = \frac{T}{T_c} \quad \text{Eq. 2.6}$$

The constants used were: T_c (CO_2)= 304.2 K; p_c (CO_2)= 73.8 bar; ω (acentric factor)= 0.228; R (gas constant)= $8.314\cdot10^{-2}$ $dm^3\cdot bar\cdot K^{-1}\cdot mol^{-1}$.

The partial pressure of CO_2 was determined using the Henry Law described by the Equation 2.7.

$$p_{CO_2} = k_h \cdot x_{CO_2} \quad \text{Eq. 2.7}$$

The k_h values were obtained from literature [65] using the empirical Equation 2.8.

$$H(T) = -0.017037T^2 + 6.1553T + 78.227 \quad \text{Eq. 2.8}$$

The values of CO_2 solubility in water were obtained from literature [63] and modelled using PE software [70].

3.3. Error analysis

Standard deviation error (u) was determined for all the obtained results. All weighing was made considering a u(*m*)=0.1 mg. For all different dissolution conditions in the wheat straw pre-treatment, the applied temperature demonstrated a u(*T*)=1 ^{o}C and pressure showed a u(p)=1 bar. An arbitrary error of 10% of measured value was defined to all the FTIR measurements and HPLC analyzes.

3.4. Kinetics modeling

The several models to analyze the xylan, glucan, arabinoxylan and acetyl groups behavior were developed based on the models presented in literature [71].

3.4.1. Fitting of data

The fitting of the experimental data to the predicted models was used to determine the reaction rate constants. The last were calculated by minimization of the sum of squares of differences between the concentrations predicted by the model equations and the experimental data using commercial software with a built-in optimization routine based on Newton's method [72].

3.4.2. Model 1

Model 1 presents the conversion of hemicellulosic xylan in autohydrolysis and CO_2-assisted autohydrolysis pretreatment to oligosaccharides, monomer sugars, furfural and further products of degradation. This model was established based on the model for brewery's spent grain presented in literature [71]. The first step of the process is the conversion of solid xylan to the potentially soluble one that at the same time hydrolyzes to XOS. Thus, the biomass kinetics is made according to the Equation 2.9, where xylan

hydrolysis is followed by 3 consecutive reactions, where the third and fourth steps are usually not desirable.

$$\text{Xylan} \xrightarrow{k'_1} \text{XOS} \xrightarrow{k'_2} \text{xylose} \xrightarrow{k'_3} \text{furfural} \xrightarrow{k'_4} \text{degradation products} \qquad \text{Eq.2.9}$$

In the case of the first step, xylan hydrolysis to XOS can be defined as shown in Equation 2.10, where k'_1 is the rate constant, [Xn], [CO_2] and [H_2O] are the xylan, CO_2 and H_2O concentrations and σ, φ, τ the order of reaction.

$$-\frac{d[Xn]}{dt} = r_1 = k'_1[Xn]^{\sigma}[CO_2]^{\varphi}[H_2O]^{\tau} \qquad \text{Eq.2.10}$$

Because either CO_2 or H_2O are used in the large excess in comparison to xylan and their concentrations with time changes insignificantly, the reaction kinetics can be expressed according to Equation 2.11, where k_1 is the pseudo-order rate constant and is presented in Equation 2.12. In this case, first-order kinetics was assumed once reaction stoichiometry is $1:1$.

$$-\frac{d[Xn]}{dt} = k_1[Xn] \qquad \text{Eq.2.11}$$

$$k_1 = k'_1[CO_2]^{\varphi}[H_2O]^{\tau} \qquad \text{Eq.2.12}$$

Integrating with [Xn_{t0}]=[Xn_0] and t=0 give the Equation 2.13, where the subscript 0 corresponds to the beginning of the isothermal conditions (when 180 ^{o}C were reached).

$$[Xn] = [Xn_0]e^{-k_1 t} \qquad \text{Eq.2.13}$$

Though, because xylan concentration can only be measured in the resultant solids thus Equation 2.13 can be written as function of solid fraction, as it is shown in Equation 2.14, where β is related to α and represents the soluble fraction of the unreacted xylan when t=0. The parameter α is the susceptible fraction, which can be calculated according to the Equation 2.16, where [Xn_{tmax}] corresponds to the remaining concentration in the solid for the longest pretreatment.

$$[Xn] = \beta[Xn_0]e^{-k_1 t} + (1-\beta)[Xn_0] \qquad \text{Eq.2.14}$$

$$\beta = 1 - (1-\alpha)\frac{100}{[Xn_0]} \qquad \text{Eq.2.15}$$

$$\alpha = \frac{100 - [Xn_{t_{max}}]}{100} \qquad \text{Eq.2.16}$$

XOS can form high and low molecular weight xylooligosaccharides, XOS_H and XOS_L respectively [56]. Therefore, the reaction sequence defined in Equation 2.9 is described

more correctly by the Equation 2.17. In the case of XOS_H, Equations 2.18 and 2.19 can be used to define XOS_H behavior during the reaction.

$$\text{Xylan} \xrightarrow{k_1} XOS_H \xrightarrow{k_2} XOS_L \xrightarrow{k_3} \text{xylose} \xrightarrow{k_4} \text{furfural} \xrightarrow{k_5} DP \quad \text{Eq.2.17}$$

$$-\frac{d[XOS_H]}{dt} = k_1[Xn] - k_2[XOS] \quad \text{Eq.2.18}$$

$$[XOS_H] = \frac{k_1\beta[Xn_0]}{k_2 - k_1}e^{-k_1 t} + \left([XOS_0] - \frac{k_1\beta[Xn_0]}{k_2 - k_1}\right)e^{-k_2 t} \quad \text{Eq.2.19}$$

For other species formed in the reaction, the equations become more complex but evolving always the same variables. Thus, for an easier comprehension, constants C_1 to C_{16} were used, as proposed by Carvalheiro et al. [56].

$$C_1 = \beta[Xn_0] \quad \text{Eq.2.20}$$

$$C_2 = (1-\beta)[Xn_0] \quad \text{Eq.2.21}$$

$$[Xn] = C_1 e^{-k_1 t} + C_2 \quad \text{Eq.2.22}$$

$$C_3 = \frac{k_1 C_1}{k_2 - k_1} \quad \text{Eq.2.23}$$

$$C_4 = [XOS_{H0}] - C_3 \quad \text{Eq.2.24}$$

$$[XOS_H] = C_3 e^{-k_1 t} + C_4 e^{-k_2 t} \quad \text{Eq.2.25}$$

$$C_5 = \frac{k_2 C_3}{k_3 - k_1} \quad \text{Eq.2.26}$$

$$C_6 = \frac{k_2 C_4}{k_3 - k_1} \quad \text{Eq.2.27}$$

$$C_7 = [XOS_{L0}] - C_5 - C_6 \quad \text{Eq.2.28}$$

$$[XOS_L] = C_5 e^{-k_1 t} + C_6 e^{-k_2 t} + C_7 e^{-k_3 t} \quad \text{Eq.2.29}$$

$$C_8 = \frac{k_3 C_5}{k_4 - k_1} \quad \text{Eq.2.30}$$

$$C_9 = \frac{k_3 C_6}{k_4 - k_2} \quad \text{Eq.2.31}$$

$$C_{10} = \frac{k_3 C_7}{k_4 - k_3} \quad \text{Eq.2.32}$$

$$C_{11} = [Xyl_0] - C_8 - C_9 - C_{10} \quad \text{Eq.2.33}$$

$$[Xyl] = C_8 e^{-k_1 t} + C_9 e^{-k_2 t} + C_{10} e^{-k_3 t} + C_{11} e^{-k_4 t} \quad \text{Eq.2.34}$$

$$C_{12} = \frac{k_4 C_8}{k_5 - k_1} \quad \text{Eq.2.35}$$

$$C_{13} = \frac{k_4 C_9}{k_5 - k_2} \quad \text{Eq.2.36}$$

$$C_{14} = \frac{k_4 C_{10}}{k_5 - k_3} \quad \text{Eq.2.37}$$

$$C_{15} = \frac{k_4 C_{11}}{k_5 - k_4} \quad \text{Eq.2.38}$$

$$C_{16} = [F_0] - C_{12} - C_{13} - C_{14} - C_{15} \quad \text{Eq.2.39}$$

$$[F] = C_{12} e^{-k_1 t} + C_{13} e^{-k_2 t} + C_{14} e^{-k_3 t} + C_{15} e^{-k_4 t} + C_{16} e^{-k_5 t} \quad \text{Eq.2.40}$$

For degradation products (e.g. formic acid), once they represent the last step and do not react to create further substances, their concentration were calculated by the material balance of xylan-derived products, according to Equation 2.41.

$$[DP] = 100 - [Xn] - [XOS_H] - [XOS_L] - [Xyl] - [F] \quad \text{Eq.2.41}$$

3.4.3. Model 2

Although glucan hydrolysis is not desirable during CO_2-assisted autohydrolysis, small amount of glucan residues as well as its degradation products might be found in the liquor phase. The conversion of glucan to degradation products with all intermediate steps occurs according to the Equation 2.42.

$$\text{Glucan} \xrightarrow{l_1} \text{GOS} \xrightarrow{l_2} \text{glucose} \xrightarrow{l_3} \text{HMF} \xrightarrow{l_4} \text{degradation products} \quad \text{Eq.2.42}$$

Model 2 was developed on the base of model 1 and was used to forecast glucan products behavior during the reaction. The Equations 2.43-2.66 present the model 2 applied.

$$C_{17} = \beta[Gn_0] \quad \text{Eq.2.43}$$

$$C_{18} = (1 - \beta)[Gn_0] \quad \text{Eq.2.44}$$

$$\beta = 1 - (1 - \alpha)\frac{100}{[Gn_0]} \quad \text{Eq.2.45}$$

$$\alpha = \frac{100 - [Gn_{t_{max}}]}{100} \quad \text{Eq.2.46}$$

$$[Gn] = C_{17} e^{-l_1 t} + C_{18} \quad \text{Eq.2.47}$$

$$C_{19} = \frac{l_1 C_{17}}{l_2 - l_1} \quad \text{Eq.2.48}$$

$$C_{20} = [GOS_{H0}] - C_{19} \quad \text{Eq.2.49}$$

$$[GOS_H] = C_{19} e^{-l_1 t} + C_{20} e^{-l_2 t} \quad \text{Eq.2.50}$$

$$C_{21} = \frac{l_2 C_{19}}{l_3 - l_1} \quad \text{Eq.2.51}$$

$$C_{22} = \frac{l_2 C_{20}}{l_3 - l_1} \quad \text{Eq.2.52}$$

$$C_{23} = [GOS_{L0}] - C_{21} - C_{22} \quad \text{Eq.2.53}$$

$$[GOS_L] = C_{21}e^{-l_1 t} + C_{22}e^{-l_2 t} + C_{23}e^{-l_3 t} \quad \text{Eq.2.54}$$

$$C_{24} = \frac{l_3 C_{21}}{l_4 - l_1} \quad \text{Eq.2.55}$$

$$C_{25} = \frac{l_3 C_{22}}{l_4 - l_2} \quad \text{Eq.2.56}$$

$$C_{26} = \frac{l_3 C_{23}}{l_4 - l_3} \quad \text{Eq.2.57}$$

$$C_{27} = [Glc_0] - C_{24} - C_{25} - C_{26} \quad \text{Eq.2.58}$$

$$[Glc] = C_{24}e^{-l_1 t} + C_{25}e^{-l_2 t} + C_{26}e^{-l_3 t} + C_{27}e^{-l_4 t} \quad \text{Eq.2.59}$$

$$C_{28} = \frac{l_4 C_{24}}{l_5 - l_1} \quad \text{Eq.2.60}$$

$$C_{29} = \frac{l_4 C_{25}}{l_5 - l_2} \quad \text{Eq.2.61}$$

$$C_{30} = \frac{l_4 C_{26}}{l_5 - l_3} \quad \text{Eq.2.62}$$

$$C_{31} = \frac{l_4 C_{27}}{l_5 - l_4} \quad \text{Eq.2.63}$$

$$C_{32} = [F_0] - C_{28} - C_{29} - C_{30} - C_{31} \quad \text{Eq.2.64}$$

$$[HMF] = C_{28}e^{-l_1 t} + C_{29}e^{-l_2 t} + C_{30}e^{-l_3 t} + C_{31}e^{-l_4 t} + C_{32}e^{-l_5 t} \quad \text{Eq.2.65}$$

Only negligible quantities of degradation products (e.g. levulinic acid) appeared in liquor phase nevertheless the step for degradation products was also took into account and can be described in the following manner:

$$DP = 100 - [Gn] - [GOS_H] - [GOS_L] - [Glc] - [HMF] \quad \text{Eq.2.66}$$

3.4.4. Model 3

Model 1 assumes that furfural and subsequent products are formed due to the xylose's degradation. However it cannot be forgotten that some furfural might also has an origin in arabinose. For this reason, kinetics based on the junction of these two compounds (arabinoxylan) was also examined. As observed below in the Equation 2.67 and in the constants C_{33} to C_{48}, the model is the similar to the first one, only changing the concentration variables.

$$ArXn \xrightarrow{k_1} AXOS_H \xrightarrow{k_2} AXOS_L \xrightarrow{k_3} AX \xrightarrow{k_4} F \xrightarrow{k_5} DP \quad \text{Eq.2.67}$$

$$C_{33} = \beta[ArXn_0] \quad \text{Eq.2.68}$$

$$C_{34} = (1 - \beta)[ArXn_0] \quad \text{Eq.2.69}$$

$$\beta = 1 - (1 - \alpha)\frac{100}{[\mathrm{ArXn_0}]} \quad \text{Eq.2.70}$$

$$\alpha = \frac{100 - [\mathrm{ArXn_{t_{max}}}]}{100} \quad \text{Eq.2.71}$$

$$C_{35} = \frac{k_1 C_{33}}{k_2 - k_1} \quad \text{Eq.2.72}$$

$$C_{36} = [\mathrm{AXOS_{H0}}] - C_{35} \quad \text{Eq.2.73}$$

$$[\mathrm{AXOS_H}] = C_{35}e^{-k_1 t} + C_{36}e^{-k_2 t} \quad \text{Eq.2.74}$$

$$C_{37} = \frac{k_2 C_3}{k_3 - k_1} \quad \text{Eq.2.75}$$

$$C_{38} = \frac{k_2 C_4}{k_3 - k_1} \quad \text{Eq.2.76}$$

$$C_{39} = [\mathrm{AXOS_{L0}}] - C_{37} - C_{38} \quad \text{Eq.2.77}$$

$$[\mathrm{AXOS_L}] = C_{37}e^{-k_1 t} + C_{38}e^{-k_2 t} + C_{39}e^{-k_3 t} \quad \text{Eq.2.78}$$

$$C_{40} = \frac{k_3 C_{37}}{k_4 - k_1} \quad \text{Eq.2.79}$$

$$C_{41} = \frac{k_3 C_{38}}{k_4 - k_2} \quad \text{Eq.2.80}$$

$$C_{42} = \frac{k_3 C_{39}}{k_4 - k_3} \quad \text{Eq.2.81}$$

$$C_{43} = [\mathrm{AX_0}] - C_{40} - C_{41} - C_{42} \quad \text{Eq.2.82}$$

$$[\mathrm{AX}] = C_{40}e^{-k_1 t} + C_{41}e^{-k_2 t} + C_{42}e^{-k_3 t} + C_{43}e^{-k_4 t} \quad \text{Eq.2.83}$$

$$C_{44} = \frac{k_4 C_{40}}{k_5 - k_1} \quad \text{Eq.2.84}$$

$$C_{45} = \frac{k_4 C_{41}}{k_5 - k_2} \quad \text{Eq.2.85}$$

$$C_{46} = \frac{k_4 C_{42}}{k_5 - k_3} \quad \text{Eq.2.86}$$

$$C_{47} = \frac{k_4 C_{43}}{k_5 - k_4} \quad \text{Eq.2.87}$$

$$C_{48} = [\mathrm{F_0}] - C_{44} - C_{45} - C_{46} - C_{47} \quad \text{Eq.2.88}$$

$$[\mathrm{F}] = C_{44}e^{-k_1 t} + C_{45}e^{-k_2 t} + C_{46}e^{-k_3 t} + C_{47}e^{-k_4 t} + C_{48}e^{-k_5 t} \quad \text{Eq.2.89}$$

$$\mathrm{DP} = 100 - [\mathrm{ArXn}] - [\mathrm{AXOS_H}] - [\mathrm{AXOS_L}] - [\mathrm{AX}] - [\mathrm{F}] \quad \text{Eq.2.90}$$

3.4.5. Model 4

As already stated, acetic acid formation along the reaction might have some influence on the reaction kinetics due to the pH lowering. Thus, model 4 is used to predict the evolution of the acetyl groups (AcO) and acetic acid (AcOH) present in the solid and liquid phases, respectively. In this case, it is assumed that acetyl groups directly hydrolyze

to form acetic acid. Accordingly, Equation 2.91 defines the percentage of remaining AcO in the solid residue, while Equation 2.92 predicts degree of the initial AcO in the liquor in the acetic acid form.

$$[\mathrm{AcO}] = [\mathrm{AcO_0}]\mathrm{e}^{-\mathrm{m_1}} \quad \text{Eq.2.91}$$

$$[\mathrm{AcOH}] = 100 - [\mathrm{AcO}] \quad \text{Eq.2.92}$$

4. Results

4.1. High pressure processes

In order to obtain experimental data for kinetics modeling, wheat straw pre-treatment was performed using different initial reaction pressures (20, 35 and 50 bar) at isothermal conditions (180 ^{o}C) from 0 to 45 minutes. Because the presence of CO_2 aims to improve autohydrolysis process, series of pre-treatments without CO_2 (autohydrolysis) were also performed.

4.1.1. Liquors' composition

The composition of liquors obtained in all experiments is shown in Tables 4.1 to 4.4 for 50, 35, 20 and 0 bar reactions, respectively. The presented tables depict concentration of all compounds found using HPLC. In general, the results produced for performed reactions show that a mixture of sugars mainly xylose both in monomeric (xylose) and oligomeric (XOS) forms was found. Additionally, cellulose as glucose monomers and oligomers were detected as well. Arabinan content was found in the samples in lower concentrations.

Table 4.1 – Liquor composition ($g \cdot L^{-1}$) for 50 bar of CO_2 initial pressure experiments.

Time (min)	0	4	6	12	18	20	25	30	35	45
log R_0	2.56	3.10	3.23	3.49	3.64	3.68	3.78	3.85	3.92	4.02
CS_{PCO2}	-1.16	-0.64	-0.49	-0.25	-0.09	-0.05	0.07	0.14	0.19	0.30
Estimated pH						3.72				
Final pH	4.46	4.38	4.37	4.11	3.94	3.99	3.92	3.62	3.73	3.64
	Composition ($g \cdot L^{-1}$)									
GOS	4.37	3.65	3.53	3.89	4.25	3.55	3.72	3.43	2.54	2.77
XOS	7.32	10.52	11.41	14.76	13.76	12.26	12.00	7.93	5.16	3.44
AOS	1.57	1.87	1.63	1.17	1.16	0.44	0.87	0.23	0.29	0.21
Glucose	0.81	0.80	0.55	0.61	0.62	0.62	0.48	1.24	0.56	0.87
Xylose	1.30	1.53	1.38	1.90	2.67	2.53	2.94	5.00	4.58	5.65
Arabinose	1.02	1.11	0.93	1.15	1.14	1.19	0.92	1.35	0.62	0.67
Acetic Acid	0.57	0.87	0.82	1.33	1.61	1.61	1.69	2.27	2.07	2.69
HMF	0.00	0.03	0.04	0.08	0.11	0.11	0.13	0.24	0.22	0.39
Furfural	0.00	0.00	0.10	0.45	0.71	0.68	1.04	2.20	2.44	3.40
Formic Acid	0.00	0.34	0.15	0.50	0.48	0.67	0.52	0.36	0.82	1.10

Table 4.2 – Liquor composition ($g \cdot L^{-1}$) for 35 bar of CO_2 initial pressure experiments.

Time (min)	0	4	8	12	16	20	25	30	40
log R_0	2.54	3.09	3.33	3.48	3.59	3.69	3.78	3.85	3.97
CS_{PCO2}	-1.25	-0.70	-0.45	-0.30	-0.19	-0.10	0.00	0.08	0.19
Estimated pH					3.78				
Final pH	4.50	4.33	4.23	4.22	3.92	3.90	3.65	3.66	3.58
	Composition ($g \cdot L^{-1}$)								
GOS	4.43	3.77	4.30	4.58	4.48	4.10	3.98	2.70	3.23
XOS	7.00	11.37	13.75	13.51	13.46	10.74	9.36	6.22	5.91
AOS	1.47	1.71	1.42	1.04	1.30	0.86	0.58	0.30	0.44
Glucose	0.37	0.63	0.63	0.52	0.26	0.60	0.35	0.66	0.62
Xylose	1.25	1.39	1.69	2.05	2.09	3.06	3.30	4.44	4.59
Arabinose	0.70	0.98	1.18	1.37	0.99	1.15	0.77	0.77	0.67
Acetic Acid	0.64	0.88	1.10	1.33	1.61	1.64	1.74	2.36	2.38
HMF	0.02	0.04	0.04	0.07	0.09	0.11	0.15	0.17	0.26
Furfural	0.00	0.10	0.10	0.21	0.64	0.87	0.87	1.31	2.21
Formic Acid	0.20	0.24	0.31	0.38	0.55	0.48	0.71	0.92	0.95

Table 4.3 – Liquor composition ($g \cdot L^{-1}$) for 20 bar of CO_2 initial pressure experiments.

Time (min)	0	4	8	12	16	20	25	30	40
log R_0	2.51	3.09	3.33	3.48	3.59	3.69	3.77	3.85	3.97
CS_{PCO2}	-1.28	-0.70	-0.45	-0.30	-0.19	-0.09	0.00	0.07	0.20
Estimated pH					3.78				
Final pH	4.35	4.04	3.95	3.85	3.80	3.60	3.60	3.60	3.53
	Composition ($g \cdot L^{-1}$)								
GOS	3.85	4.23	4.19	3.53	4.59	3.40	3.46	3.48	3.00
XOS	7.24	10.23	13.10	12.53	11.80	11.20	9.68	7.55	4.21
AOS	1.50	1.66	1.22	1.07	1.03	0.79	0.68	0.60	0.44
Glucose	0.66	0.51	0.44	0.47	0.72	0.62	0.61	0.54	0.76
Xylose	1.23	1.36	1.70	2.30	3.42	3.32	3.80	4.31	5.30
Arabinose	0.74	1.03	1.34	1.08	0.99	0.94	0.83	0.69	0.63
Acetic Acid	0.86	1.02	1.22	1.51	1.63	1.77	1.81	2.22	2.60
HMF	0.01	0.02	0.04	0.07	0.49	0.11	0.14	0.19	0.28
Furfural	0.02	0.07	0.18	0.55	0.59	1.19	1.05	1.59	3.10
Formic Acid	0.25	0.34	0.38	0.49	0.51	0.62	0.64	0.79	0.91

Table 4.4 – Liquor composition ($g \cdot L^{-1}$) for autohydrolysis experiments.

Time (min)	0	4	8	12	16	20	25	30	40
log R_0	2.74	3.20	3.39	3.52	3.63	3.71	3.80	3.87	3.99
CS_{PCO2}	-2.76	-2.30	-2.11	-1.98	-1.87	-1.79	-1.70	-1.63	-1.51
Final pH	4.48	4.40	4.15	4.02	4.07	3.93	3.78	3.80	3.73
	Composition ($g \cdot L^{-1}$)								
GOS	4.54	4.42	4.70	4.42	4.11	4.53	3.99	3.98	3.75
XOS	5.49	8.74	12.08	13.22	13.62	13.45	13.05	12.36	9.35
AOS	1.60	1.65	1.68	1.64	1.40	1.19	0.89	0.84	0.59
Glucose	0.37	0.52	0.63	0.35	0.33	0.32	0.29	0.37	0.48
Xylose	1.24	1.29	1.34	1.31	1.69	2.29	2.43	2.93	4.20
Arabinose	0.61	0.98	1.07	1.14	1.07	1.12	1.03	1.06	0.91
Acetic Acid	0.67	0.85	1.00	1.17	1.43	1.61	1.87	2.11	2.26
HMF	0.01	0.02	0.04	0.04	0.06	0.08	0.10	0.12	0.17
Furfural	0.00	0.03	0.09	0.15	0.36	0.57	0.80	1.19	1.89
Formic Acid	0.15	0.21	0.26	0.32	0.36	0.43	0.43	0.57	0.73

The obtained results allow to conclude either reaction time and pressure exerted influences the liquor composition. For the same pressure used e.g. 50 bar it can be stated that, the XOS concentration increases during the first minutes of isothermal process and next followed by a decrease with reaction progress. At 50 bar of initial reactions pressure, the maximal XOS concentration was detected at the level of 14.76 $g \cdot L^{-1}$ after 12 minutes of isothermal treatment. For longer reaction times the decay of XOS concentration was accentuated and led to production of xylose and furfural and after 45 minutes of isothermal reaction, the XOS concentration was as high as 3.44 $g \cdot L^{-1}$, which was counterbalanced by 5.65 $g \cdot L^{-1}$ of xylose and 3.40 $g \cdot L^{-1}$ of furfural. The mono and oligomers of arabinose were observed in liquor. The profiles for AOS and arabinose were similar to those for XOS and xylose respectively, however due to the significantly lower concentration of arabinan in untreated biomass, the concentration of both arabinose in monomeric and oligomeric forms are as low as 0.21 $g \cdot L^{-1}$ and 0.67 $g \cdot L^{-1}$ after 45 minutes of the reaction carried out at 50 bar of initial pressure. Glucan hydrolysis was also observed in all reactions however the concentrations of GOS and glucose are almost constant and varies from 4.37 $g \cdot L^{-1}$ to 2.77 $g \cdot L^{-1}$ for GOS and from 0.81 $g \cdot L^{-1}$ to 0.87 $g \cdot L^{-1}$ for glucose along the reaction time. The concentration of HMF along the reaction progress increases however even after 45 minutes is still low (0.39 $g \cdot L^{-1}$).

Another important compound formed during the reaction is acetic acid. Its concentration increases over time but shows a tendency to stabile the concentration for prolonged reaction time (2.69 $g \cdot L^{-1}$). Another organic acid found in the liquors was formic acid. The concentration of formic acid is generally lower than 1 $g \cdot L^{-1}$ and its trend is similar to those observed for acetic acid.

The profiles of the aforementioned products along the time of reaction carried out at 50 bar of initial pressure are depicted in Figure 4.1.

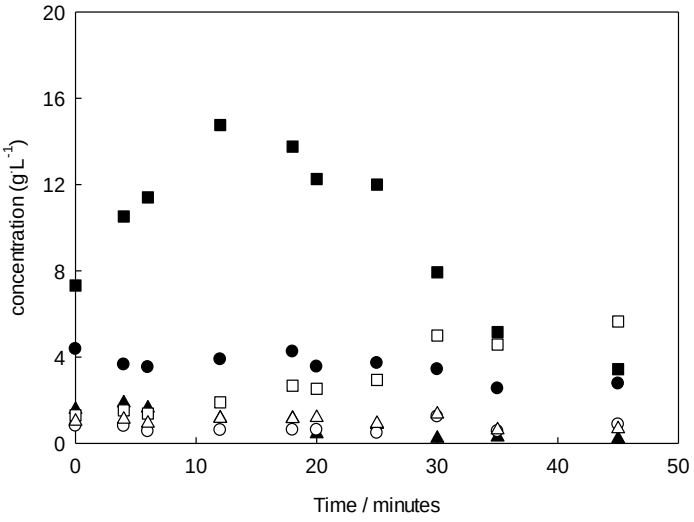

Figure 4.1 – The saccharides' profiles (● – GOS, ○ – glucose, ■ – XOS, □ – xylose, ▲ – AOS, △ – arabinose) as a function of time of reaction carried out at 50 bar of initial pressure. Formic acid, acetic acid, furfural and HMF were omitted for clarity of the figure.

Considering the influence of pressure on the reaction products, it can be stated that higher CO_2 pressure guides to higher XOS concentration which decays with time to lower values than in case of lower pressures. For comparison, XOS concentration at 50 bar has maximum as high as 14.76 $g \cdot L^{-1}$ and decreases to 3.44 $g \cdot L^{-1}$ after 45 minutes while for the 20 bars of initial pressure, the XOS concentration peaks at 13.10 $g \cdot L^{-1}$ and fall down to 4.21 $g \cdot L^{-1}$ after 40 minutes. Additionally, the xylose concentrations for the same pressures achieve 5.65 $g \cdot L^{-1}$ and 5.30 $g \cdot L^{-1}$ for 50 and 20 bar initial pressures. Similar tendency is observed in case of another product originated in pentoses such as furfural. The concentration of furfural is higher for higher initial pressure (3.40 $g \cdot L^{-1}$ for 50 bar) and decreases to 3.10 $g \cdot L^{-1}$ for 20 bar. As it was before discussed, the AOS and arabinose

concentrations are relatively low, however it can be seen that higher initial pressure favors insignificantly the AOS to arabinose. GOS and glucose concentrations as well as HMF formation are less dependent on the exerted pressure during reaction. For example, for 35 bar and 0 (autohydrolysis) bar the concentration of GOS is only slightly higher in case of autohydrolysis reaction than for 35 bar, which on the other hand is counterbalanced by higher concentration of glucose and HMF at higher reaction pressures. At 35 bar and at 40 minutes of the reaction time, the GOS, glucose and HMF concentrations are 3.23 $g \cdot L^{-1}$, 0.62 $g \cdot L^{-1}$ and 0.26 $g \cdot L^{-1}$, while for autohydrolysis the same compounds have the following concentrations: 3.75 $g \cdot L^{-1}$, 0.48 $g \cdot L^{-1}$ and 0.17 $g \cdot L^{-1}$. In case of formic acid it can be seen that higher initial pressure favors strongly its concentration. This effect is not so pronounced for acetic acid. For example for autohydrolysis, the concentrations either acetic or formic acids are as high as 2.26 $g \cdot L^{-1}$ and 0.73 $g \cdot L^{-1}$, while for 50 bars, the aforementioned acids have the concentrations as high as 2.69 $g \cdot L^{-1}$ and 1.10 $g \cdot L^{-1}$ respectively.

Another important aspect of the produced liquid fraction rich in formic and acetic acids as well as in-situ created carbonic acid from CO_2 dissolved in water is a pH. In case of autohydrolysis it is observed that longer reaction time lowers pH of the formed liquor from 4.48 to 3.73 (for 0 and 40 minutes of isothermal treatments) mostly due to the increase of organic acids concentration up to 0.73 $g \cdot L^{-1}$ and 2.25 $g \cdot L^{-1}$ for formic and acetic acids respectively. Considering the CO_2 processes it can be found that estimated pH is significantly lower than actually measured pH after the depressurization. The difference is more pronounced for the highest examined pressure (3.72 and 4.46 for estimated and measured pHs). The difference between both pHs (estimated and measured) decreases along the reaction time and for the longest processes the measured pH is even lower than estimated one obtained from the van Walsum equation [65] for all examined initial pressures.

Besides saccharides, organic acids and furanic compounds, the produced liquors was also subject to capillary electrophoresis analyses to determine phenolic compounds, e.g. vanillin. Figure 4.2 represents the relation between the area of total phenolics, reaction time and initial reaction pressure. It is visible that prolonged reaction time as

well as higher pressures reduces the concentration of phenolics but for prolonged reaction times and higher initial pressures a small increase of total phenolics is observed. Figure 4.3, the area of vanillin is presented as function of time for various reaction pressures. As it can be seen in Figure 4.3 the increase of the reaction time increases the area of vanillin and this increase is superior in case of higher pressures than in case of autohydrolysis.

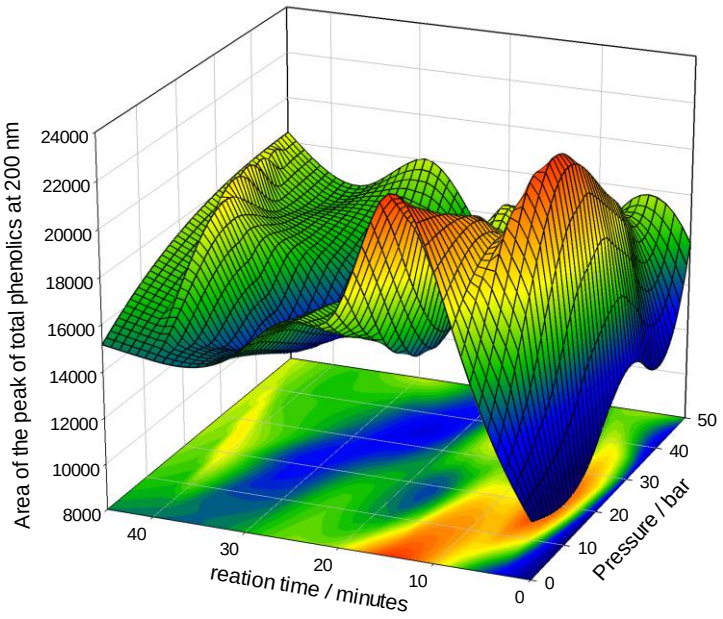

Figure 4.2 –Dependence of peak area of total phenolics on reaction time and pressure.

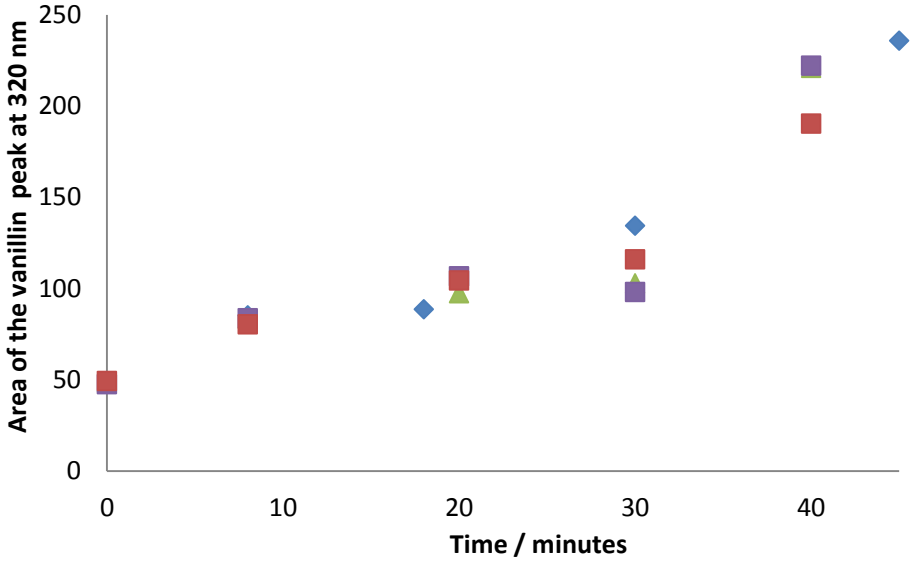

Figure 4.3 – Vanillin formation as a function of time for various initial pressures (red – autohydrolysis; purple – 20 bar; green – 35 bar; blue – 50 bar).

4.2. Processed solids' composition

To evaluate pre-treatment effectiveness, resulting solids were subject to composition analysis. To perform this, treatment mentioned above was performed and obtained samples were analyzed by HPLC. This allowed to determine the composition of solids as well as to evaluate the sugar's removal in comparison to the untreated feedstock. Tables 4.5-4.8 present the evolution of processed solid's composition (weight percentage) in terms of glucan, xylan, arabinan, acetyl groups and Klason lignin for all the pre-treatments performed.

Similarly to the feedstock composition and due to relatively low concentration of GOS, glucose and HMF in the liquor, glucan represents the main fraction in the processed solids. In general, for constant initial pressure, e.g. 35 bar of CO_2 the glucan contents increases in the first minutes of the isothermal process and later stabilizes reaching around 50% of the processed solid content. In case of xylan, its concentration decreases gradually and achieves the concentration as low as 3.52 wt.% of processed solid at 35 bar of initial pressure. Either arabinan and acetyl groups were found in very low amount in the processed solid (1.28 and 3.00 wt.%) at the beginning of the isothermal processes at 35 bar and their concentration is progressively decaying achieving a complete removal of arabinan and only 1.38 wt.% of acetyl groups after 40 minutes of isothermal processes at 180 ^{o}C at initial pressure of 35 bar of CO_2. As Klason lignin is the less affected by the reaction conditions therefore the Klason lignin content increases with time of the process and reaches 1/3 of the processed solid composition for 35 bar of CO_2 of initial pressure.
Other important aspect is the solid yield which along the isothermal process decreases from 90.72 wt.% to 2/3 of the initial biomass loading after 40 minutes at 35 bar of initial CO_2 pressure. Analogous observation can be done for all examined pressures (either autohydrolysis or 20 or 50 bar of CO_2) as it is depicted in Tables 4.5-4.8.

Analyzing the pressure influence on xylan concentration in the processed biomass, it can be stated that higher reaction pressure in general favors removal of xylan, especially for longer reaction times, however for the intermediate ones the differences between 50 bar and autohydrolysis are less visible. In other words, for intermediate reaction times the xylan concentration was the lowest for both middle pressures' studied

(20 and 35 bar of CO_2). In numbers it can be given in the following way: 6.07 wt.%, 6.66 wt.%, 8.03 wt.% and 9.75 wt.% for 20, 35, 50 and 0 bar of initial pressure respectively for 20 minutes. It is important to add that as the absolute values for the examined pressures are relatively similar or even in the range of experimental error, thus it is difficult to find a clear trend for xylan content as a function of pressure for intermediate reaction time. For longer reaction times at steady state conditions (40-45 minutes of isothermal process) the xylan content follows the expected trend. It means, the xylan concentration is the lowest at 50 bar of initial pressure (2.84 wt.%) and increases to 3.52 wt.% (35 bar), 3.67 wt.% (20 bar) up to 5.82 wt.% for autohydrolysis as it can be observed in Figure 4.4.

On the other hand, the highest glucan content was observed in case of autohydrolysis reaction after 40 minutes (52.00 wt.%) and decreases gradually up to 48.19 wt.% for reaction carried out at 50 bar of CO_2 of initial pressure after 45 minutes. In case of Klason lignin it can be stated that higher pressure increases the lignin content in processed solid from 30.72 wt.% for autohydrolysis to 34.79 wt.% in case of 50 bar of initial pressure. Either arabinan or acetyl groups were found in such small quantities (no more than 4.40 wt.% in total) in biomass thus, a clear dependence between pressures exerted during the isothermal treatment and concentration of both compounds is difficult to be established. The same cannot be said about the solid yield which is clearly a function of pressure used in the reaction. Higher pressure decreases the solid yield either at the beginning of the reaction (t=0) or at the steady state conditions (t=40 or 45 minutes). For example at the beginning of the isothermal process the solid yield for 50 bar was the lowest and reached 88.96 wt.%, while with the decrease of the pressure, the solid yield increased to 92.77 wt.% for autohydrolysis. The same dependence is visible for steady state conditions for which a autohydrolysis process permitted to achieve 69.03 wt.% of solid yield and it decreases to yield as low as 65.50 wt.% for 50 bar of initial CO_2 pressure isothermal reaction.

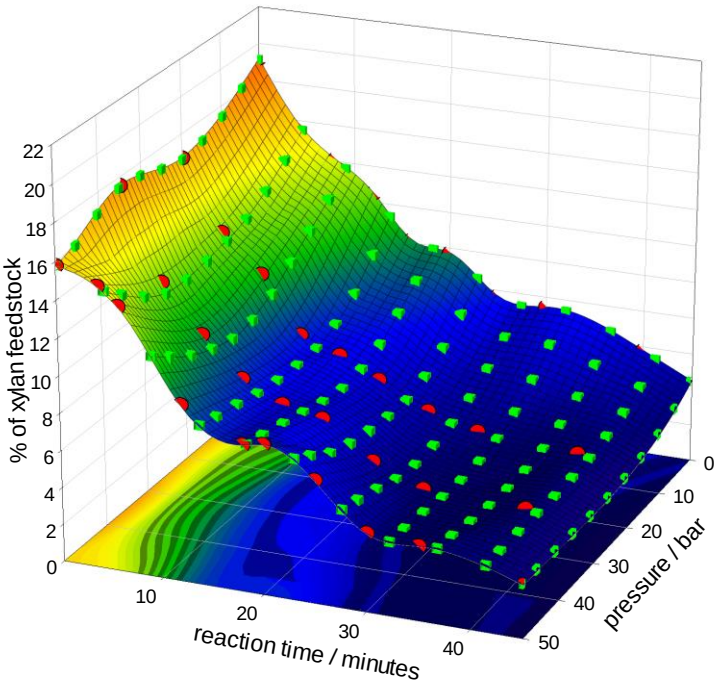

Figure 4.4 – Xylan content in processed biomass as a function of time and pressure exerted during the isothermal treatment.

Table 4.5 – Solid residues composition for 50 bar of CO_2 initial pressure reactions.

Time (min)	0	4	6	12	18	20	25	30	35	45
Solid yield	88.96	92.78	91.03	67.18	73.75	66.91	72.30	60.37	80.11	65.50
	Composition ($g \cdot 100\ g^{-1}$)									
Glucan	40.91	44.45	45.63	50.46	50.89	49.39	50.41	51.33	53.72	48.19
Xylan	15.78	15.01	14.12	9.45	7.84	8.03	6.58	4.21	3.98	2.84
Arabinan	1.33	1.05	1.06	0.53	0.62	0.54	0.53	0.11	0.45	0.00
Acetyl Groups	2.72	2.56	2.53	1.75	1.55	1.56	1.39	1.17	1.12	1.03
Klason Lignin	19.69	20.59	22.23	26.19	27.54	27.62	28.11	32.11	31.74	34.79

Table 4.6 – Solid residues composition for 35 bar of CO_2 initial pressure reactions.

Time (min)	0	4	8	12	16	20	25	30	40
Solid yield	90.72	89.20	87.02	63.94	68.80	69.70	67.44	67.24	66.90
	Composition ($g \cdot 100\ g^{-1}$)								
Glucan	41.44	46.73	49.48	49.11	51.03	49.25	51.95	52.47	48.24
Xylan	17.56	12.72	10.21	8.15	7.10	6.66	4.76	3.69	3.52
Arabinan	1.28	0.76	0.30	0.11	0.10	0.15	0.00	0.00	0.00
Acetyl Groups	3.00	2.38	2.19	1.78	1.76	1.64	1.44	1.33	1.38
Klason Lignin	20.43	23.18	24.92	27.14	28.47	29.77	30.96	32.06	33.01

Table 4.7 – Solid residues composition for 20 bar of CO_2 initial pressure reactions.

Time (min)	0	4	8	12	16	20	25	30	40
Solid yield	92.85	70.87	72.47	67.04	64.60	68.66	67.73	65.77	67.57
	Composition ($g \cdot 100\ g^{-1}$)								
Glucan	40.35	44.46	47.51	47.71	48.59	51.10	49.34	51.21	51.90
Xylan	16.70	12.94	10.95	7.92	7.11	6.07	4.75	4.04	3.67
Arabinan	1.41	0.58	0.31	0.13	0.10	0.01	0.00	0.00	0.00
Acetyl Groups	2.82	2.33	1.91	1.64	1.56	1.43	1.22	1.10	1.08
Klason Lignin	20.85	22.62	23.61	26.22	27.59	28.43	30.99	31.50	32.69

Table 4.8 – Solid residues composition for autohydrolysis reactions.

Time (min)	0	4	8	12	16	20	25	30	40
Solid yield	92.77	83.73	75.35	74.43	71.35	65.50	67.04	66.86	69.03
	Composition ($g \cdot 100\ g^{-1}$)								
Glucan	38.67	42.51	45.40	49.96	43.46	49.78	51.37	49.85	52.00
Xylan	19.18	15.91	14.12	12.52	10.18	9.75	7.69	7.47	5.82
Arabinan	1.67	0.84	0.48	0.30	0.30	0.25	0.05	0.00	0.00
Acetyl Groups	2.73	2.05	1.72	1.26	1.22	0.98	0.80	0.72	0.56
Klason Lignin	20.98	21.91	23.66	25.26	25.83	28.05	28.34	30.01	30.72

4.3. Kinetics modeling

According to published results, all the analyzed reactions can be modelled assuming irreversible and pseudo-first order kinetics model [56, 73, 74]. For the modelling purposes the obtained data for liquid and solid samples were normalized to presented to corresponding models in the function of xylan, arabinoxylan, glucan and acetyl groups in the scale 0-100% of each fraction composition. Thus the results of modelling are depicted in figures 4.5 to 4.16. Calculated rate constants and R^2 are presented in the Tables 4.9 to 4.11. Data was fitted to the reaction sequence, applying the Equations 2.9 to 2.92.

4.3.1. Model 1

Model 1 was created to predict xylan evolution along the reaction. The correlation factors presented in the Table 4.9 shows a very good agreement between the experimental data and model predictions.

Table 4.9 – Kinetic constants obtained for model 1.

Initial pressure (bar)	0	20	35	50
α	0.8203	0.8678	0.8737	0.9002
k_1 (min^{-1})	0.0926	0.1271	0.1090	0.0726
k_2 (min^{-1})	0.0411	0.0641	0.0647	0.0677
k_3 (min^{-1})	0.0411	0.0641	0.0647	0.0677
k_4 (min^{-1})	0.0534	0.0566	0.0621	0.0596
k_5 (min^{-1})	0.0431	0.0409	0.0500	0.0395
$[XOS_H]$ ($g \cdot L^{-1}$)	20.36	22.73	28.61	32.90
R^2 Xn	0.9986	0.9937	0.9873	0.9611
R^2 XOS	0.9924	0.9701	0.9370	0.9058
R^2 Xyl	0.9440	0.9335	0.9175	0.7865
R^2 F	0.9788	0.9289	0.9713	0.9431
R^2 DP	0.9412	0.8844	0.8049	0.8280

The obtained data shows that for higher pressure the susceptive xylan fraction is dependent on pressure exerted during reactions. For autohydrolysis α is as high as 0.82 while for 50 bar is 0.90. The reaction rate constants are also a function of pressure, however this relation is not a straightforward for reactions with and without CO_2. Considering the k_1 for CO_2-asssited reactions the k_1 decreases from 0.1271 min^{-1} to 0.0726 min^{-1} with the increase of pressure from 20 to 50 bar. In case of autohydrolysis reaction, k_1 was as high as 0.0926 min^{-1}. The reaction rate constants of subsequent reactions (k_2, k_3) are less pressure dependent and in general the presence of CO_2 increases the k's values by 50% in comparison to autohydrolysis. For k_4 and k_5 the function of reaction rate constant is practically independent on the pressure exerted during the reaction.

Another important aspect, referred also in literature [56], is that after xylan hydrolysis, high and low molecular weight XOS are produced, but determination techniques used in the present study did not allow to perform the distinction of this concentration and measured [XOS] are the sum of $[XOS_H]$ and $[XOS_L]$. To model $[XOS_H]$ and $[XOS_L]$ Equations 2.25 and 2.29 were used, optimizing k_2 and k_3 simultaneously to the parameter $[XOS_{H0}]$, where $[XOS_{L0}]$ was calculated by difference between $[XOS_0]$ and $[XOS_{H0}]$. Thus, as this parameter has a physical effect and present the concentration of high molecular weight XOS it can be stated that foreseen concentration of high-molecular weight XOS is increasing with the pressure increase.

Figures 4.5-4.8 depict the results of the model 1 application for xylan removal and its hydrolysis products' formation as a function of time for 50, 35, 20 bar of initial pressure and autohydrolysis.

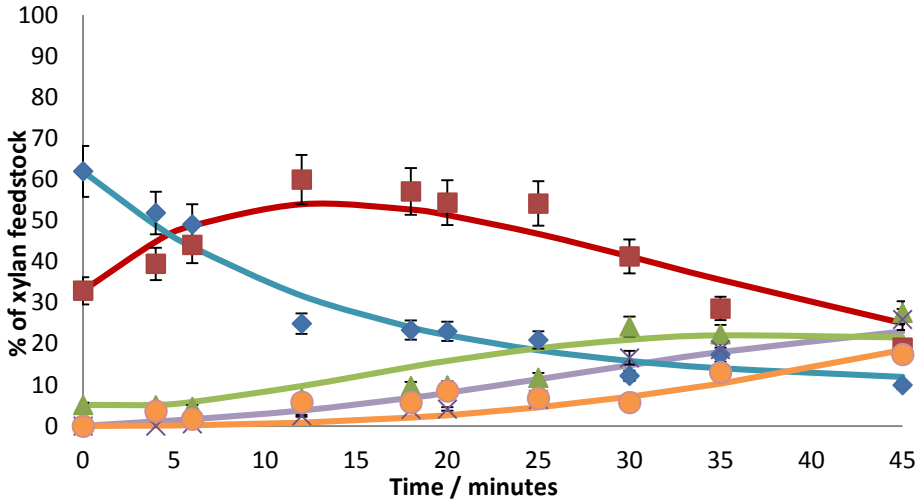

Figure 4.5 – Xylan removal and resulting products as function of time for 50 bar reactions. Experimental data (Dots) and model (solid lines): blue – xylan remaining in the residue; red – xylan in the form of XOS; green – xylan converted into xylose; purple – xylan in the form of furfural; orange – degradation products from xylan.

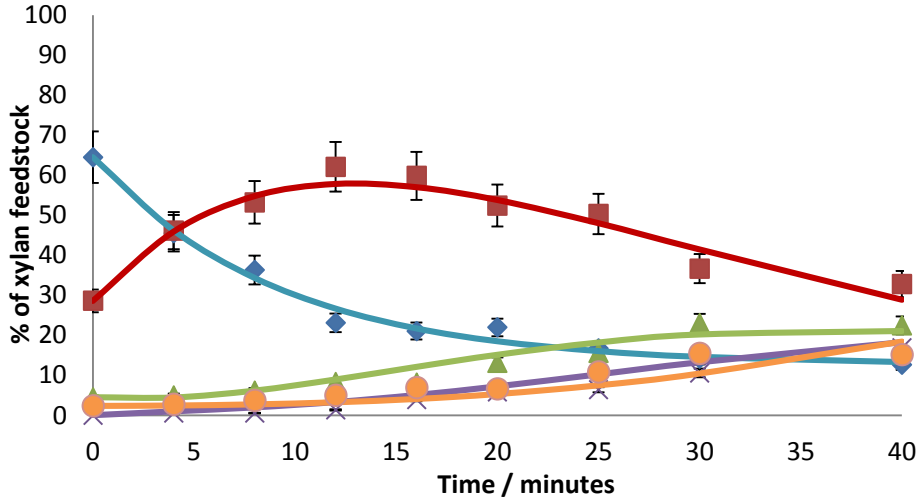

Figure 4.6 – Xylan removal and resulting products as function of time for 35 bar reactions. Experimental data (Dots) and model (solid lines): blue – xylan remaining in the residue; red – xylan in the form of XOS; green – xylan converted into xylose; purple – xylan in the form of furfural; orange – degradation products from xylan.

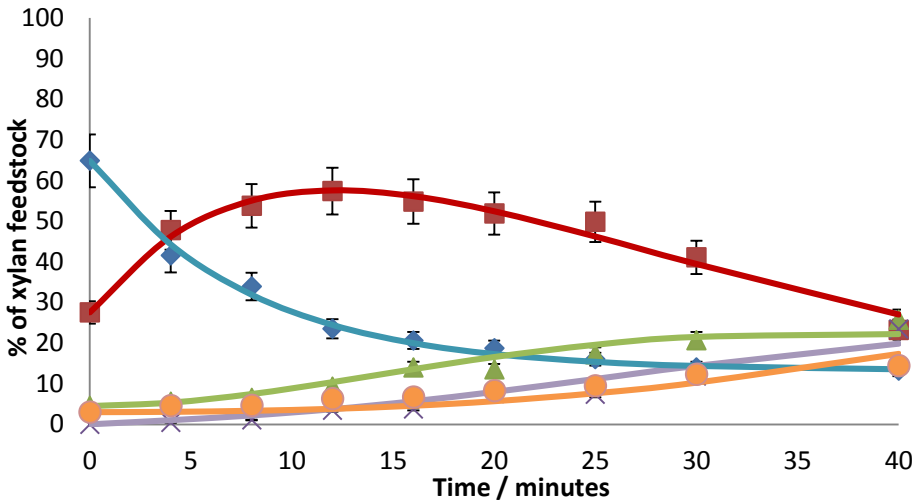

Figure 4.7 – Xylan removal and resulting products as function of time for 20 bar reactions. Experimental data (Dots) and model (solid lines): blue – xylan remaining in the residue; red – xylan in the form of XOS; green – xylan converted into xylose; purple – xylan in the form of furfural; orange – degradation products from xylan.

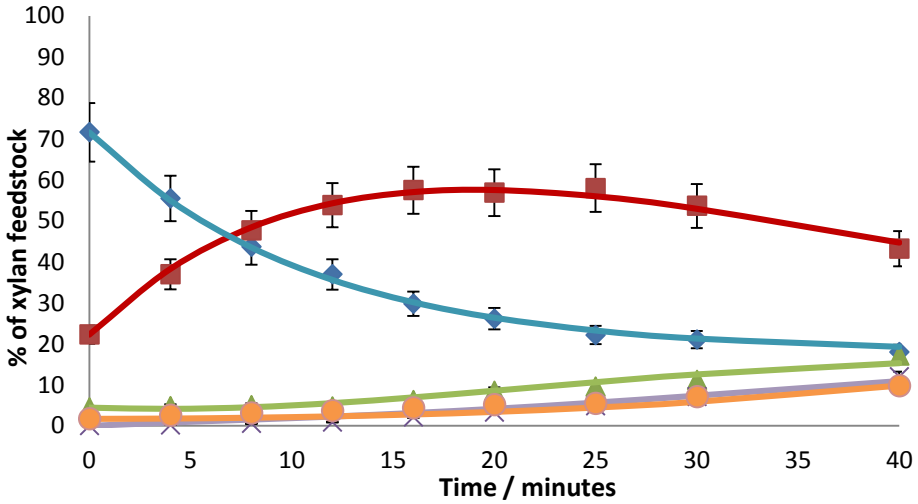

Figure 4.8 – Xylan removal and resulting products as function of time for autohydrolysis reactions. Experimental data (Dots) and model (solid lines): blue – xylan remaining in the residue; red – xylan in the form of XOS; green – xylan converted into xylose; purple – xylan in the form of furfural; orange – degradation products from xylan.

4.3.2. Model 2

Model 2 was based on model 1 and was developed to forecast the glucan behavior. However the obtained results demonstrate that concentration of glucan as well as other

products of glucan conversion are practically time independent for all examined reaction conditions.

4.3.3. Model 3

Model 1 assumes the formation of furfural solely by the xylose degradation. However, due to the arabinan presence in the feedstock some furfural can be produced from this saccharide. Thus, to improve the accuracy of model 1, model 3 considers arabinoxylan fraction. All the results are presented in Figures 4.9 to 4.13 and Table 4.10. The results of this model shows that values of α are slightly higher than in case of model 1 and additionally, all reaction rate constants are very similar to those obtained in model 1. Furthermore, the model 3 approximate better experimental results than model 1 once the worst R^2 is higher as 0.82 while in model 1 the worst one was as low as 0.78.

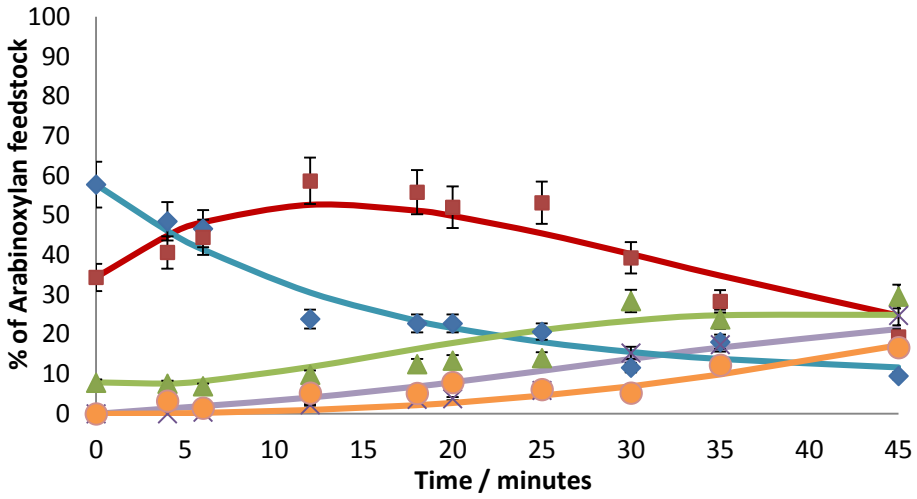

Figure 4.9 – Arabinoxylan removal and resulting products as function of time for 50 bar reactions. Experimental data (Dots) and model (solid lines): blue – arabinoxylan remaining in the residue; red –AXOS; green – AX; purple – Furfural; orange – DP.

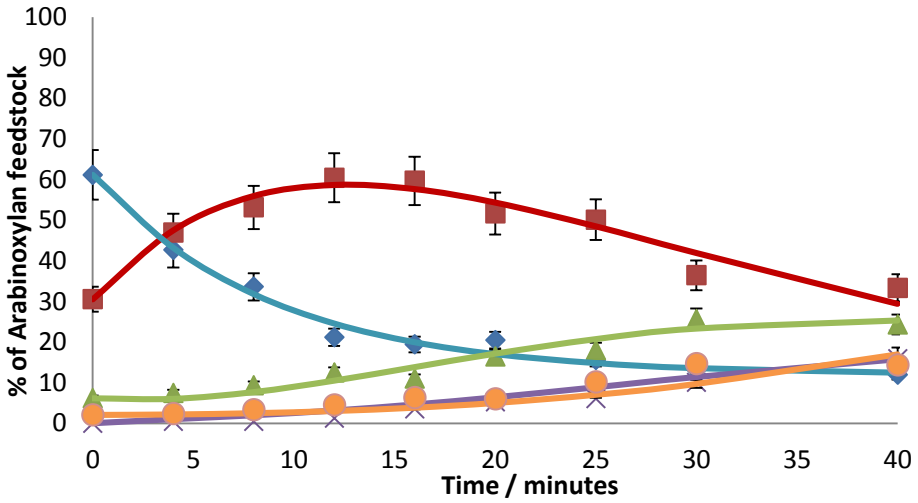

Figure 4.10 – Arabinoxylan removal and resulting products as function of time for 35 bar reactions. Experimental data (Dots) and model (solid lines): blue – arabinoxylan remaining in the residue; red –AXOS; green – AX; purple – Furfural; orange – DP.

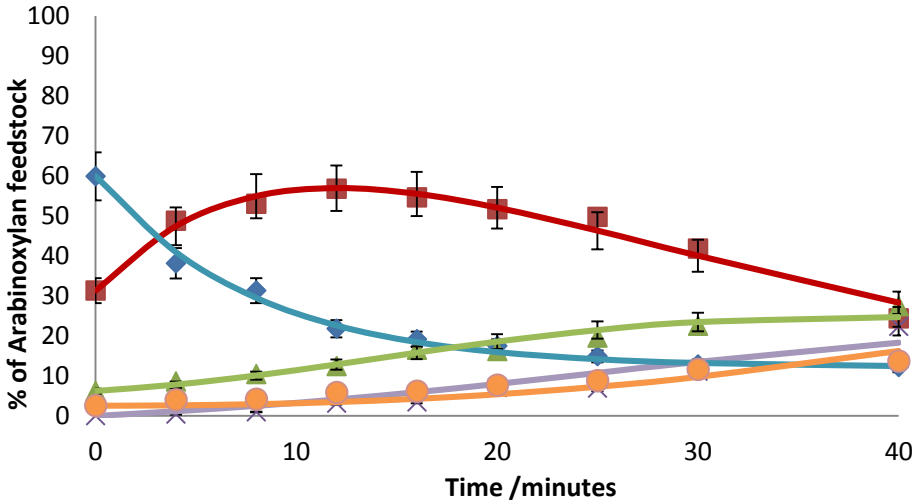

Figure 4.11 – Arabinoxylan removal and resulting products as function of time for 20 bar reactions. Experimental data (Dots) and model (solid lines): blue – arabinoxylan remaining in the residue; red –AXOS; green – AX; purple – Furfural; orange – DP.

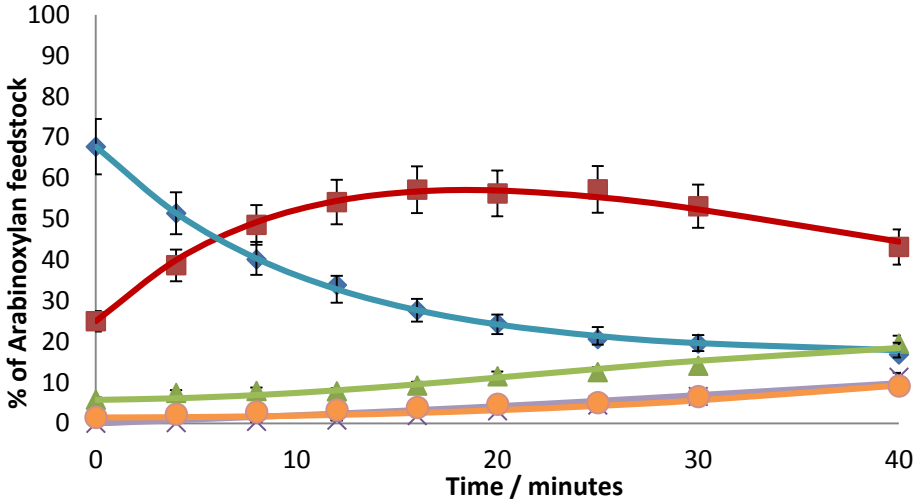

Figure 4.12 – Arabinoxylan removal and resulting products as function of time for 20 bar reactions. Experimental data (Dots) and model (solid lines): blue – arabinoxylan remaining in the residue; red –AXOS; green – AX; purple – Furfural; orange – DP.

Table 4.10 – Kinetic constants obtained using model 3.

Initial pressure (bar)	0	20	35	50
α	0.8314	0.8784	0.8802	0.9042
k_1 (min^{-1})	0.0964	0.1267	0.1134	0.0692
k_2 (min^{-1})	0.0387	0.0594	0.0630	0.0666
k_3 (min^{-1})	0.0387	0.0594	0.0620	0.0666
k_4 (min^{-1})	0.0382	0.0461	0.0471	0.0481
k_5 (min^{-1})	0.0433	0.0403	0.0527	0.0385
$[AXOS_H]$ ($g \cdot L^{-1}$)	17.71	20.86	30.57	34.37
R^2 ArXn	0.9989	0.9929	0.9870	0.9512
R^2 AXOS	0.9917	0.9644	0.9299	0.9075
R^2 AX	0.9613	0.9515	0.9294	0.8207
R^2 F	0.9558	0.9131	0.9692	0.9318
R^2 DP	0.9559	0.9037	0.8160	0.8472

4.3.4. Model 4

In model 4, acetyl group's hydrolysis as well as acetic acid formation was predicted. Experimental data and kinetic model's prediction are presented in the Figures 4.13 to 4.16 and Table 4.11, where a good correlation between both data is presented and R^2 are always above 0.9491. In this model it is assumed that acetyl groups directly hydrolyze into

acetic acid, thus as the time increases and the acetyl groups' concentration decays in the solid fraction, acetic acid increases in the liquor.

The reaction rate constant is pressure dependent and its value decreases with the pressure increase from 0.0480 min^{-1} for autohydrolysis to m_1=0.0345 min^{-1} for 50 bar assays.

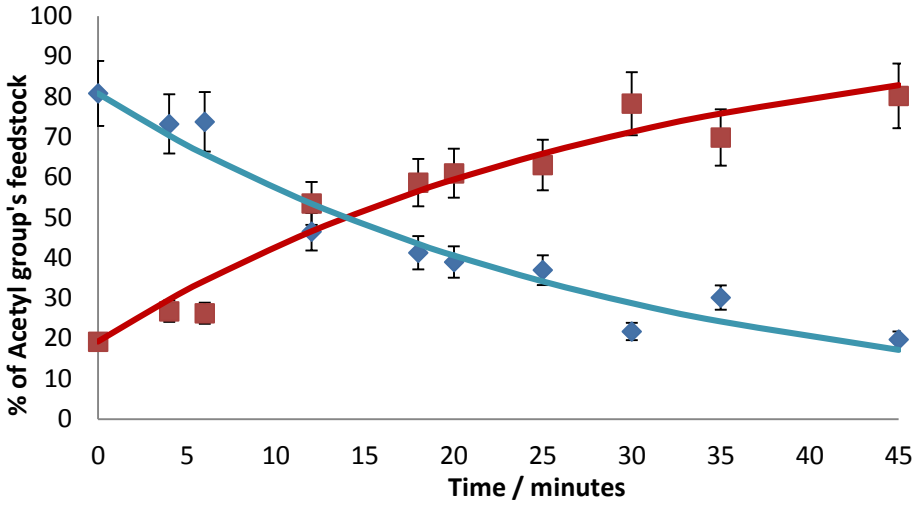

Figure 4.13 – Acetyl group's removal and acetic acid as function of time for 50 bar reactions. Experimental data (dots) and model (solid lines): blue – acetyl groups remaining in the residue; red – acetic acid.

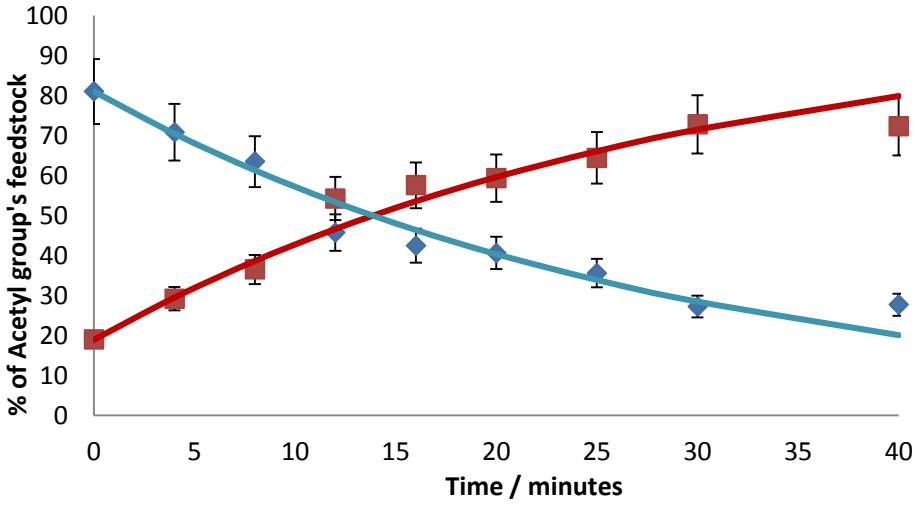

Figure 4.14 – Acetyl group's removal and acetic acid as a function of time for 35 bar reactions. Experimental data (dots) and model (solid lines): blue – acetyl groups remaining in the residue; red – acetic acid.

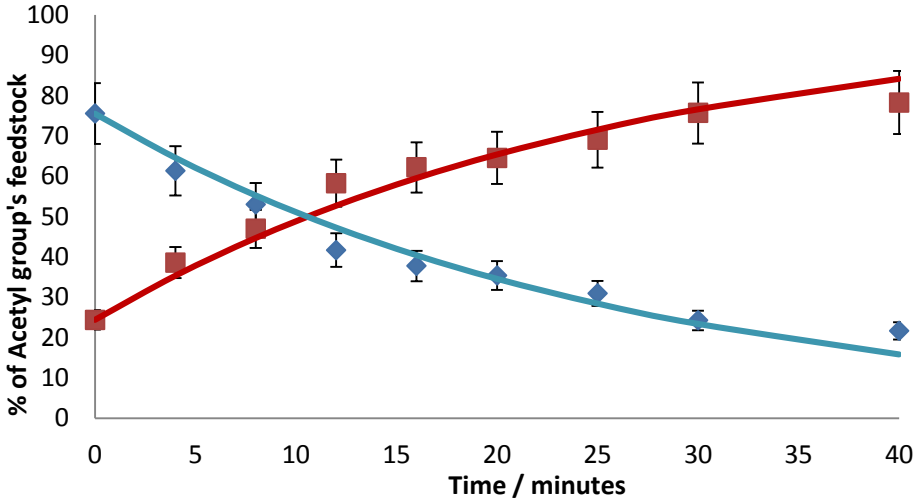

Figure 4.15 – Acetyl group's removal and acetic acid as a function of time for 20 bar reactions. Experimental data (dots) and model (solid lines): blue – acetyl groups remaining in the residue; red – acetic acid.

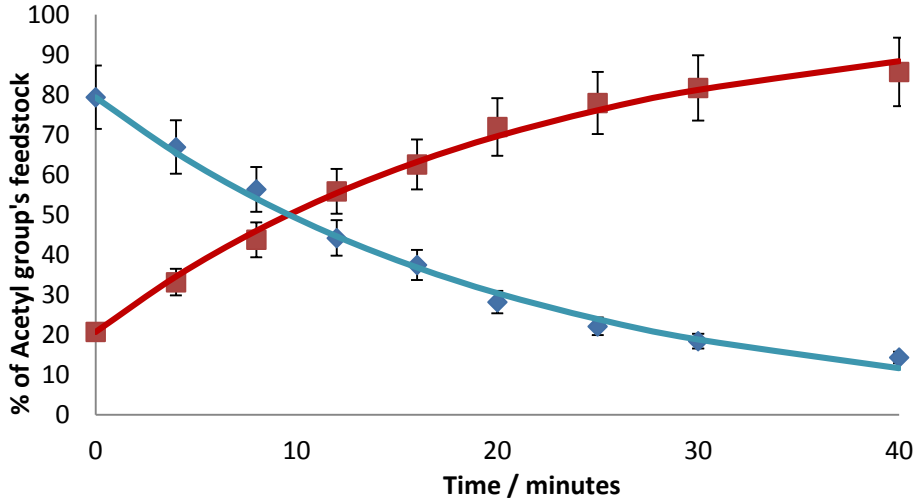

Figure 4.16 – Acetyl group's removal and acetic acid as a function of time for autohydrolysis reactions. Experimental data (dots) and model (solid lines): blue – acetyl groups remaining in the residue; red – acetic acid.

Table 4.11 - Kinetic constants obtained using model 4.

Initial pressure (bar)	0	20	35	50
m_1 (min^{-1})	0.0480	0.0391	0.0348	0.0345
R^2 AcOH	0.9946	0.9770	0.9569	0.9491
R^2 AcO	0.9946	0.9770	0.9569	0.9491

5. Discussion

5.1. The high pressure pre-treatments

5.1.1. The liquors' composition

The obtained results for all examined pressures show the previously observed behavior either for autohydrolysis or CO_2-assisted processes [38, 54, 56, 75]. A dominant products found in liquors are xylooligosaccharides. In general, the concentration of XOS picks and later decreases with the reaction time and is counterbalanced by the formation of XOS hydrolysis product such as xylose or further degradation to furfural. The highest registered concentration of XOS was 14.76 $g \cdot L^{-1}$ and is 1 $g \cdot L^{-1}$ lower than those obtained by Magalhães da Silva et al. for process at 210 ^oC at 60 bar of CO_2 [38]. Thus the results presented in this work are only slightly worse than the literature ones but on the other hand were obtained at more energetically beneficial conditions (30 ^oC and 10 bar of CO_2 lower). Comparing this result to autohydrolysis data [54], it can be stated that the presence of CO_2 guides to produce almost 50% more XOS than in autohydrolysis at the maximal concentration (215 ^oC). For similar $logR_0$ (3.50), the difference between concentrations is even higher and is 6.09 vs. 14.76 $g \cdot L^{-1}$ for autohydrolysis and CO_2 processes, respectively. Sipponen found that in case of autohydrolysis the total sugar released at optimal $logR_0 = 3.81$ was 66% of arabinoxylan that is in a good agreement with the data produced in this work (69%). The beneficial effect of CO_2 on the XOS production originates in the carbonic acid formation in the presence of water [58, 61, 65]. Even at relatively low pressure of CO_2 at 180 ^oC the water phase contains 0.01 mole fraction of CO_2 [63] contributing to lowering pH of the produced solution. Similar behavior can be found for 35 bar of initial pressure where the maximal concentration of XOS was as high as 13.75 $g \cdot L^{-1}$. At this conditions, the final pressure achieved in the reaction was 50 bar and the solubility of CO_2 in water is even lower (xCO_2=0.007), which may affect the potential for hydrolysis of the formed medium. For the lowest examined pressure (20 bar of CO_2) the XOS concentration continue to lower and equals 13.10 $g \cdot L^{-1}$ after 8 minutes of reaction at 180 ^oC. In this case, CO_2 is practically insoluble in water thus reaction occurs in three almost immiscible system constituted by gaseous CO_2, liquor containing mostly water and solid biomass. It is interesting to observe that autohydrolysis

performed at 180 °C allowed to obtain at the maximum 13.62 g·L^{-1} of XOS. It indicates that in some cases the presence of CO_2 does not provide any benefits for the XOS production. Even in case of 35 bar of initial CO_2 pressure the concentration of XOS is identical as this for autohydrolysis but on the other hand the formed XOS might be later converted to xylose and furfural thus it is important to overview the XOS concentration together with monomeric xylose and furfural. As it was presented before in results section, the concentrations of xylose and furfural increase along the reaction time and in general, higher CO_2 pressure favors hydrolysis of XOS to xylose and later to furfural as depicted in Figure 5.1. Moreover, the presence of CO_2 accelerates the process which can be important in terms of time and energy consumption.

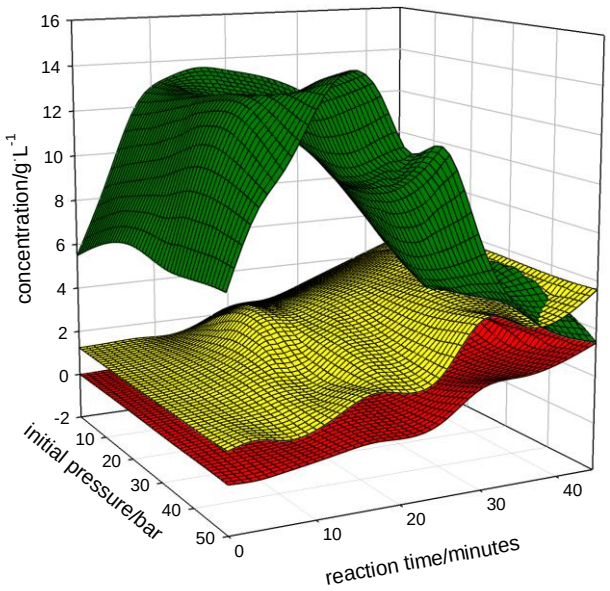

Figure 5.1 – The XOS (green), xylose (yellow) and furfural (red) concentrations in the produced liquors as a function of reaction time and initial pressure.

At 50 bar either xylose or furfural concentrations are the highest among all found in liquors (5.65 and 3.40 g·L^{-1}, respectively), while for autohydrolysis these values are much lower and equal to 4.20 and 1.89 g·L^{-1}, correspondingly. This clearly indicates that at steady state conditions, the hydrolysis of XOS to xylose and further to furfural is more advanced than in case of autohydrolysis. This finding can be confirmed by the acidity of the reaction medium. Due to the high temperature and pressure applied during reactions, the measurement of pH during the pre-treatment is impossible. In addition, because CO_2

is used in the reactions and its presence allow to form acidic conditions' *in-situ,* the acidity of the medium produced during the process can be only estimated, once these conditions are reversible when CO_2 is released. The best known method to do so is the van Walsum function [65], which is a semi-empirical relation involving the partial pressure of CO_2 in water. Unfortunately, this formula (Equation 1.5) does not foresee the influence of other formed products on the medium pH. It is especially important in case of organic acids (e.g. formic or acetic acids) formed in the course of the reaction, which may strongly modify the pH of the solution. Nevertheless, the calculated values allow to approximate the pH of the medium during the reaction and it is clear that for higher CO_2 pressure the estimated pH is slightly lower than in case of 35 or 20 bar of initial CO_2 pressure experiments. Another method to follow the pH of the reaction medium is the measurement of the pH directly after the depressurization. However this experiment does not reflect the real value due to the fact mentioned before [61]. Furthermore, these measurements have one additional error, which is mostly associated to the fact that time needed to achieve equilibrium after the depressurization is relatively long. In other words, the CO_2 dissolved in the reaction medium during reaction goes out from this solution during the depressurization however, even at ambient conditions, part of CO_2 is still soluble in water and the time needed to achieve equilibrium is dependent on many factors such as the ambient temperature, partial pressure of CO_2 in environment and CO_2 pressure used in the reaction. Although the determined pH values might be incorrect, the tendency observed for series of processes allows taking semi-quantitative conclusions. Thus, as it can be observed in Tables 4.1-4.4, the final pH measured decreases strongly with the reaction progress and in some cases the concentration of hydronium ion ($[H_3O^+]$) is one order of magnitude higher for prolonger reaction times than at the t=0. This confirms that formed products have a great impact on the pH of the reaction medium.

The less concentrated fraction of hemicellulose are acetyl groups which constitute 2.72 wt.% of initial biomass. The low pH formed by carbonic acid and by autoionization of water catalyzes the acetyl group hydrolysis and as it can be observed higher CO_2 pressure and prolonged reaction time contribute to the increase of concentration of acetic acid [76, 77]. It is especially visible in case of the reactions carried out at 50 bar of initial CO_2

pressure where between t=0 and steady state conditions, the concentration of acetic acid increases by 1.1 $g \cdot L^{-1}$. Another important fraction constituting hemicellulose is arabinan. However due to its low concentration in untreated biomass (3.02 wt.%) its concentration as AOS and arabinose in liquor is very low.

Other fraction of biomass which is susceptible to the pre-treatment conditions is cellulose. Cellulose was found in liquors as glucooligosaccharides and glucose and HMF which are produced according to Equation 2.42 and their concentration varies as depicted in Figure 5.2.

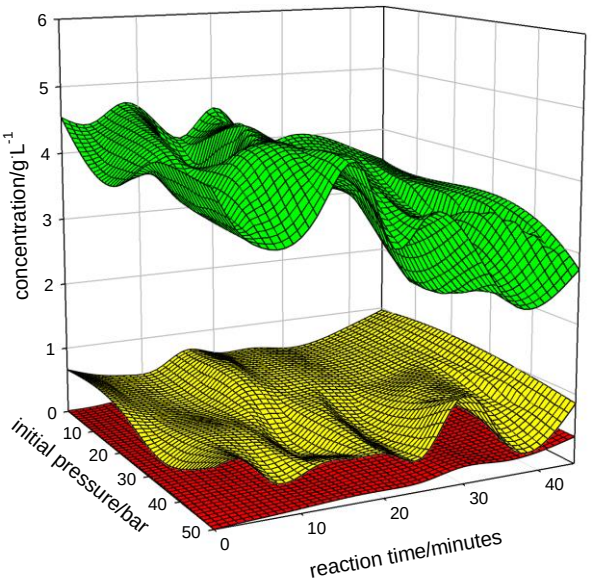

Figure 5.2 – The GOS (green), glucose (yellow) and HMF (red) concentrations in liquors as a function of reaction time and initial pressure.

Cellulose being one of the fractions more resistant for pre-treatment produces lower concentration of GOS, glucose and HMF than xylan from hemicellulose. Cellulose, as it was explained before has in the structure either amorphous or crystalline fragments. The crystalline structure is less susceptible to hydrolysis however amorphous one undergoes hydrolysis much easier. Thus, the formation of GOS, glucose and HMF might be originated in amorphous cellulose [61]. Analyzing obtained results it can be stated that the GOS concentration decreases slightly along the reaction time as it is depicted in Figure 5.2, and it is partially counterbalanced by the glucose and HMF concentrations' increase. Although the presented trends are rather clear, the influence of reaction time and

pressure are rather small and differences of concentrations are relatively low and do not exceed 0.5 $g \cdot L^{-1}$ especially for glucose and HMF. This confirms that cellulose is very rigid fraction of biomass and hydrolysis of more susceptible amorphous cellulose occurs at relatively less severe conditions, while more severe conditions (higher pressure and/or temperature) are needed to hydrolyze crystalline cellulose more efficiently [54].

The obtained liquors are rich in oligosaccharides which are one of the value added products from biomass. Oligosaccharides are known from their potential applications in food, pharmaceutical, and cosmetic industries [48]. Therefore, the aim of biomass valorization could be to obtain oligosaccharides' concentrations as high as possible. Considering XOS, GOS and AOS present in liquor, it can be stated that XOS are leading OS among all of oligosaccharides. The maximal concentration of OS was as high as 19.82 $g \cdot L^{-1}$ (Figure 5.3) and XOS constitutes ¾ of all oligosaccharides in this liquor.

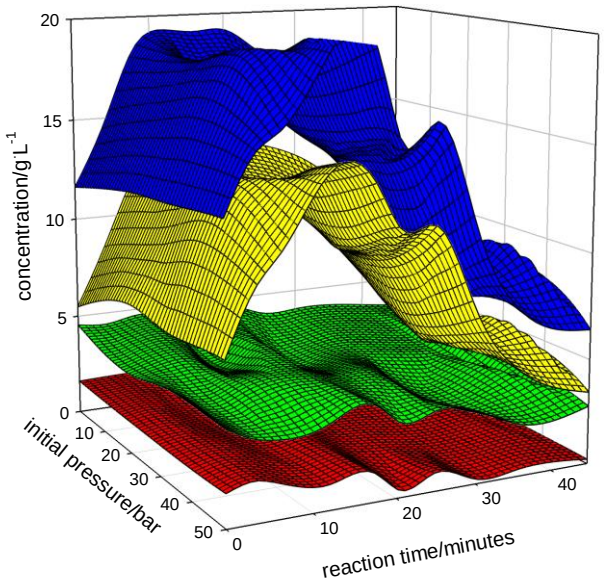

Figure 5.3 – The AOS (red), GOS (green), XOS (yellow) and OS (blue) concentrations in liquors as a function of reaction time and initial pressure.

Liquors were also a subject to the electrophoresis analysis. The electrophoresis was used to examine the presence of polyphenolics in the sample. Due to the complexity of the detected spectrum as well as impossibility to perform qualitative and quantitative analysis the semi-qualitative analysis on the base of total phenolics areas was made. The obtained data presented in Figure 4.2 shows that for lower pressures the concentration

of phenolics, (mostly phenolic acids) being formed by hydrolysis of naturally present hydroxybenzoic and cinnamic acid derivatives, peak while along the reaction time decreases with the progress of the reaction. For more severe conditions, the radicals formed from progressive degradation of phenolics can react with other simple phenolic acids and increase of total phenolics area is observed. In addition, the direct lignin degradation previously observed in literature also contribute to this effect [78]. One of the dominant phenolic compounds detected in the mixture is vanillin. Vanillin was also found previously in wheat straw after the pre-treatment with ionic liquids [6]. Magalhães da Silva discovered that for more severe reaction conditions, the concentration of vanillin as well as all phenolics increased that was also found in this work.

5.1.2. Processed solids

To complete the analysis of pre-treatment effectiveness on the biomass used, the liquid fraction must be examined together with the produced solid. Therefore, considering the previously described findings in liquors it can be stated that the results of processed solids are in good agreement with the liquor composition. The Figure 5.4 presents the three main fractions present in the processed solid as a function of pressure and reaction time.

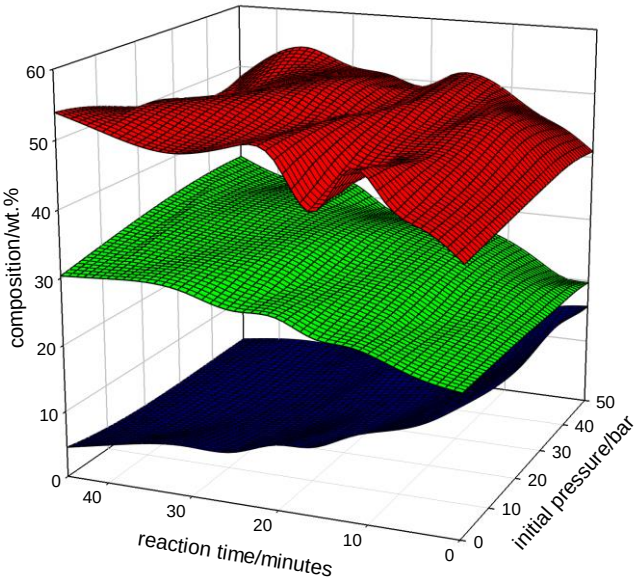

Figure 5.4 – The glucan (red), Klason lignin (green) and xylan (blue) content in the processed solids depending on reaction time and initial pressure of the reaction.

In case of xylan, most of it was hydrolyzed and was presented in the liquor phase. Similarly to the increase of xylose and furfural concentration at higher pressure and for longer isothermal process times, the xylan removal was more accentuated as it is depicted in Tables 4.5-4.8. More severe reaction conditions guided to more extended removal of xylan leaving as low as 2.84 wt.% of xylan in the processed biomass obtained after the pre-treatment at 180 °C after 45 minutes. This data are in generally good agreement with the literature ones where for the same combined severity factor (CSp_{CO_2}= 0.19), the xylan content in processed biomass was 5.95 wt.% and in this work is 5.16 wt.% [61]. As depicted in Figure 4.4 and Figure 5.3, the xylan removal decreases slightly for lower CO_2 pressures or even more for autohydrolysis. In case of autohydrolysis, the literature results show that for similar $logR_0$ = 4, the xylan content is between 5 and 10 wt.% [54], while in this work is 5.82 wt.%. Analogously to xylan removal, the complete removal of arabinan was observed especially that arabinan is known as much easier hydrolysable polysaccharide than xylan [54]. Similarly, acetyl group content in the produced solid decreases accordingly to the increase of the acetic acid concentration in the liquor reaching the content as low as 1.03 wt.% after 45 minutes of isothermal process at 50 bar of initial CO_2 pressure. This is again in a good agreement with literature results where similar range of acetyl groups were detected in processed solids [38, 54, 61]. One of the dominant fractions in the obtained solid is Klason lignin. Lignin was found mostly in liquor as polyphenols although in low concentration and because of this it can be indicated that lignin was practically unaffected by the process conditions [38, 61]. According to the results shown in Tables 4.5-4.8, the Klason lignin content increases with the reaction progress and with the rise of the exerted pressure during the reaction. It is due to the fact that results are shown as the relative concentration of each fraction in the formed solid and the enhanced xylan removal origins the increase of relative concentration of Klason lignin. Similar effect is also evident in case of glucan because among all polysaccharides presented in the biomass, glucan is less susceptible fraction to hydrolysis. This lower glucan hydrolysis was also observed in liquor composition where the concentration of GOS, glucose and HMF was significantly lower than xylan. It is even more visible considering the relative concentration of glucan

in the untreated biomass (Table 2.1), which is strongly enriched in comparison to the untreated biomass. In raw material xylan and glucan constituted 19.18 wt.% and 38.59 wt.% while in the produced solids the same fractions were found in significantly different ratio (2.84 wt.% vs. 48.19 wt.% for 45 minutes, 50 bar of initial CO_2 pressure process). The enhancement of processed solid compositions is typical for autohydrolysis reactions either with or without CO_2 and was reported in the literature [38, 54, 56, 61].

The significant removal of hemicellulose from the biomass helps in the cellulose valorization; however other parameter, such as crystallinity, inhibits it. In order to evaluate the effect of the pre-treatment on the cellulose crystallinity, three samples of solids, untreated wheat straw and processed solids after 30 min of autohydrolysis and pretreatment with CO_2 at 50 bar of initial pressure, underwent a FTIR analysis. For the cellulose crystallinity analyzes two absorption bands were selected as it was depicted before. A band at 1437 cm^{-1} is characteristic to the scissoring vibration assigned to CH_2 in the crystalline cellulose and the band at 898 cm^{-1}, assigned to C-O-C bonds of β-1,4 glycosidic bonds is typical for amorphous cellulose [79]. To compare the crystallinity, the LOI index, which is the ratio between 1437 cm^{-1} and 898 cm^{-1}, was calculated [80]. However, it is important to realize that although the sample for FTIR analyzes were prepared using exactly the same amounts of materials, the glucan content in each of them is different. In case of untreated biomass the glucan content is 38.59 wt.% while for autohydrolysis is 49.85 wt.% and 51.33 wt.% for process with CO_2. Thus, normalizing the obtained data in a function of glucan content the crystallinity results obtained from FTIR are presented in Table 5.1. At the first look, comparing the LOI it seems that untreated biomass has the lowest crystallinity (LOI=2.30) in comparison to autohydrolysis sample (3.56) and from processes carried out at 50 bar of initial CO_2 pressure (4.16).

Table 5.1 – FTIR results of solid samples, untreated wheat straw, solid residue after 30 min of autohydrolysis and pretreatment at 50 bar.

	A_{1437}	**A_{898}**	**LOI (A_{1437}/ A_{898})**
Untreated Wheat Straw	0.239	0.104	2.30
Autohydrolysis (30 min)	0.217	0.061	3.56
50 bar (30 min)	0.183	0.044	4.16

However, a close inspection of each peak shows that in case of autohydrolysis 41% of amorphous cellulose and only low amount (9%) of crystalline cellulose was removed. In case of CO_2-asssited process the removal of both types of cellulose is more effective. Amorphous cellulose continues to be removed even more efficiently (57% and 23% of amorphous and crystalline cellulose, respectively in comparison to untreated biomass). Therefore, the LOI for both pre-treatments is higher than LOI for untreated sample, while in fact crystallinity seems to be lower as in both cases amorphous cellulose was removed significantly and additionally in CO_2 process some portion of crystalline one was expelled as well [61].

5.2. Kinetics modeling

Kinetics modelling allows to follow the reaction progress as well as to analyze the evolution of the reaction products. Kinetics is either pressure or temperature dependent, however the effect of pressure on reaction rate constant for condensed-phase reactions is generally low. Nevertheless, many literature reports were published which demonstrate the importance of pressure on biomass processing [38, 61, 81, 82]. Therefore the study of kinetics even for low pressures is needed and was carried out in this work. The obtained liquor and solid fractions' composition allowed to perform the kinetics study and to model the xylan, glucan, arabinoxylan and acetyl group hydrolysis and formation of consecutive products from the mentioned fractions. All models were constructed based on the models presented in literature [71]. The results permit to conclude that even for much more complex systems, such as CO_2-assisted processes, the obtained data are well represented by the used models. As it was discussed before model 1 and 3 were used to describe the xylan and arabinoxylan conversion to xylose, furfural and degradation products. The reason for this is that furfural, the xylose degradation product, can be formed either from xylose or arabinose. Thus, the assignment of entire furfural formation to xylose degradation would be an excessive simplification of the occurring reactions in the examined systems. Analyzing of the produced values of k_4 (conversion of xylose or arabinoxylose to furfural in model 1 or 3, respectively) a decrease of the reaction rate constant from 0.0596 min^{-1} to 0.0481 min^{-1} between models is clearly observed. This is directly associated to higher concentration of arabinoxylose than xylose

for the same concentration of the same furfural produced thus reaction rate constant is lower.

One of the interesting observations for models 1 and 3 is that in both models, the k_1 is strongly dependent on reaction pressure as it is shown in Figure 5.5. Furthermore, the relation is not linear and the highest reaction rate constant for both models was observed for 20 bar of CO_2 initial pressure and the reaction rate constant decreases from 0.1271 or 0.1267 min^{-1} for models 1 or 3 respectively to 0.0726 min^{-1} and 0.0692 min^{-1} for both mentioned models for 50 bar of initial CO_2 pressure. It may indicate that higher pressure of CO_2 affects negatively the reaction kinetics or in this case particularly the hydrolysis of xylan to form XOS.

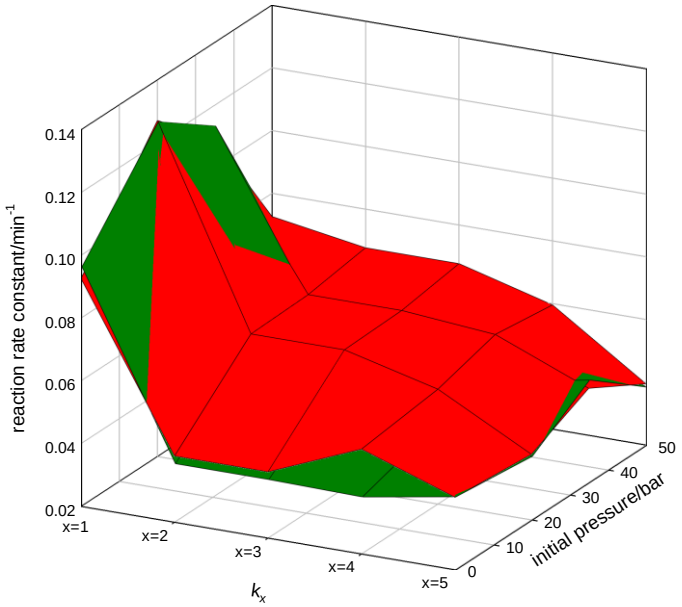

Figure 5.5 – The reaction rate constant (k_1, k_2, k_3, k_4, k_5) values (min^{-1}) as function of initial reaction pressure

To understand this behavior it is important to go back to the origin of severity factor. The severity factor roots in the kinetics of hemicellulose hydrolysis and in the applicable form, as it is shown in Equation 1.2, contains a temperature 100 ^oC. This temperature was historically established as a references temperature based on pulping processes established in 1950s [83] and was broadly used for many pre-treatment processes [48, 54, 66, 84, 85]. Above this reference temperature, the hydrolysis process begins, thus during the time needed to achieve the required temperature, in this case 180 ^oC, reaction takes place already. Accordingly, using model data, it is possible to estimate

the time when hydrolysis started and it is different for each examined reaction conditions. Because reactions were carried out with different initial CO_2 pressure (20, 35 and 50 bar) different numbers of moles of CO_2 were inserted in the system, which are proportional to the CO_2 density at the initial reaction conditions [86]. Therefore it is clear that reaction carried out at higher pressure takes more time to reach 180 ^oC and by this, time of hydrolysis is longer than since reaction mixture reaches 180 ^oC. Thus, to analyze the real effect of CO_2 it is needed to calculate the initial reaction rate taking into account this "real" reaction time. In addition, it is important to note that depending on the conditions used, different amount of arabinoxylan or xylan is susceptible to hydrolysis. These values, presented as α parameter, depict that for more severe conditions more xylan or arabinoxylan can undergo hydrolysis. Therefore, at the examined conditions never entire arabinoxylan or xylan can be hydrolyzed and only the susceptible fraction must be considered as initial arabinoxylan or xylan concentrations. Hence bearing in mind all these specificities and postulating a first order disappearance of arabinoxylan, plots of log [ArXn] versus time did show straight lines for the initial stages of the reaction as depicted in Figure 5.6.

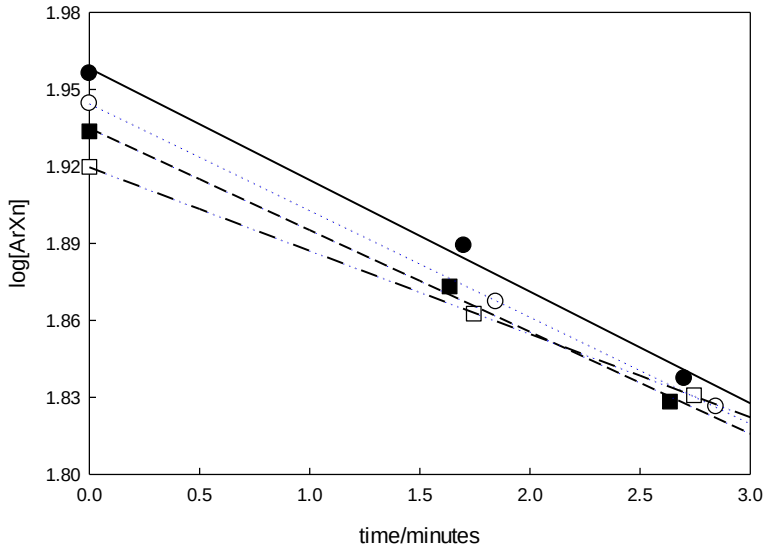

Figure 5.6 – Log [ArXn] as a function of initial reaction time for various reaction conditions (● and solid line – 50 bar of initial CO_2 pressure, ○ and dotted line – 35 bar of initial CO_2 pressure, ■ and dashed line – 20 bar of initial CO_2 pressure, □ and dashed-double dotted line – autohydrolysis reaction). Lines were linear regression to determined initial reaction rate constant.

The initial reaction rate constants, k_1, for each reaction conditions were estimated based on linear regression of data produced by the used model and are presented in Table 5.2.

Table 5.2 – The initial reaction rate constant k_1 for models 1 and 3 for examined initial pressures exerted during reactions.

Initial pressure (bar)	0	20	35	50
k_1 (min^{-1}) model 1	0.0322	0.0375	0.0411	0.0428
k_1 (min^{-1}) model 3	0.0325	0.0397	0.0416	0.0435

The attained values of initial reaction rate constant demonstrate that indeed higher reaction pressure, especially in case of CO_2 present, accelerates the xylan hydrolysis to XOS while in the overall view the relation is different as it was discussed above.

The obtained rate constant, k_1, is very similar to those calculated by Garrote et al. [85] for corncob and slightly higher (about 25%) than k_1 reported by Carvalheiro et al. [71] for brewery's spent grain, both using autohydrolysis process. On the other hand k_2 is 25% lower than found for corncob reported by Gorrote [85] but 20% higher than reported by Carvalheiro et al. [71]. The later also found the same relation between the rate constants, including that xylose degradation into furfural has a faster kinetics than the depolymerization step, having obtained the correspondent rate constant similar to those calculated in the present study. The same behavior was also observed by Gullón et al. [73] for rye straw but in this case the kinetics is much slower and the rate constant of sugar's degradation into furfural is even higher than xylose removal from biomass in reaction with liquid to solid ratio of 8 ($w \cdot w^{-1}$). Comparing this data to other pre-treatment methods it can be stated that methods presented in this work have greater capacity to remove hemicellulose fraction. For example wet oxidation method reported by Schmidt et al. [87] gave k_1=0.0580 min^{-1} at 185°C for liquid to solid ratio of 9.5 ($w \cdot w^{-1}$), corresponding only to 45% of k_1 observed for 20 bar of initial CO_2 pressure assays in this work. Guerra-Rodriguez et al. [88] found that, at optimal conditions, k_1=0.1122 using a 2% H_2SO_4 solution ($w \cdot w^{-1}$), although it was made at lower temperature (130 °C) thus it needs further neutralization and separation process to remove the acid.

Regarding the liquid part of xylan derivative conversions (XOS, xylose and furfural) it can be observed that k_2, k_3 and k_4 generally increase with the reaction pressure and only

conversion of furfural to further degradation products is almost pressure independent. A close inspection of the obtained values of reaction rate constant, k_2 and k_3, shows that both present the same value. This phenomenon was also observed in case of brewery's spent grain [71] and may indicate that the hydrolysis of XOS_H to XOS_L is independent from the degree of XOS polymerization.

The catalytic effect of medium is also evident in case of acetyl groups which hydrolysis is displayed by model 4. Similarly to behavior observed xylan or arabinoxylan, the pressure of CO_2 has a negative impact on the reaction rate. Although the difference is relatively negligible considering the established errors it can be observed that the highest rate of hydrolysis of acetyl groups to acetic acid is for autohydrolysis and later in case of CO_2 presence the reaction rate slows down. However the analysis of initial reaction rate constant shows that CO_2 has in fact a positive effect and accelerate the hydrolysis of acetyl groups and initial reaction rate constant are m_1 = 0.0157, 0.0151, 0.0147, 0.0132 min^{-1} for 50, 35, 20 bar of initial CO2 pressure and autohydrolysis, correspondingly. Thus in the graphical form the reaction rate constant and initial reaction rate constant for acetyl group hydrolysis to acetic acid can be depicted as it is illustrated in Figure 5.7.

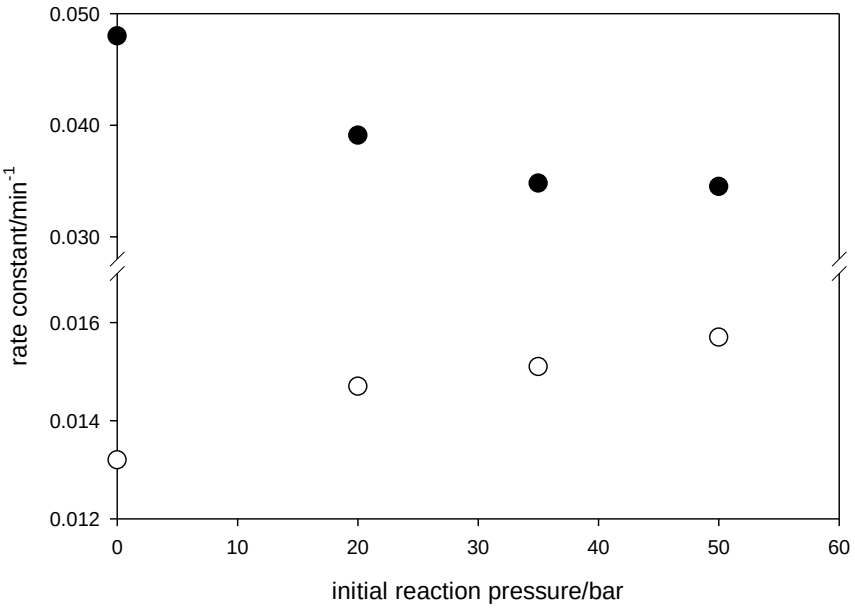

Figure 5.7 – The reaction rate constant (●) and initial reaction rate constant (○) for hydrolysis of acetyl groups to acetic acid as a function of exerted pressure during reaction.

Model 2 was used to describe the hydrolysis of glucan to GOS, glucose, HMF and further degradation products. As it was observed in case of solid and liquid phases' composition, the dependence of concentrations of each fraction along the reaction time is negligible. The concentrations of GOS, glucose and HMF in liquid phase are relatively low and do not exceed 2 $g \cdot L^{-1}$ with the exception of GOS. This data are with the agreement with the previously reported in literature [38, 54, 61]. Such low concentrations, especially for glucose and HMF, have a significant error associated to these values. Therefore the kinetic constants calculated based on this data has a large uncertainty and cannot be considered as reliable. Furthermore, reaction rate constants (l_1 to l_5) have values lower than 0.01 min^{-1}, which confirms again that glucan conversion is almost insignificant at the examined conditions.

6. Conclusions

The work developed in this study indicates that lignocellulosic biomass, in particular wheat straw, is a low-value feedstock with a great potential to produce diverse products including bulky low value biofuels, but also other small volume value-added products, namely xylooligosaccharides. In this context, biomass pretreatment plays a crucial role within biorefinery concept for a selective fractionation of the biomass, especially hemicellulose fraction.

Carbon dioxide provides additional catalytic conditions to autohydrolysis process, improving xylan and arabinan hydrolysis kinetics affecting cellulose minimally. This way a solid richer in glucan and Klason lignin might be more suitable for further valorization helping to complete the biorefinery concept.

The proposed kinetic models predicted the irreversible pseudo-first-order kinetic models allowed to calculate the rate constants. The experimental data were accurately projected by the proposed models. The R^2 was generally higher than 0.9 and only is some particular cases was lower, however considering the complexity of the performed experiments, especially with CO_2, and analysis of the produced fractions it can be stated that obtained results are reliable.

7. Perspectives for future work

The developed studies allowed to achieve series of interesting results presented in this work. However to complete this work some additional research listed below can be done.

1) Other less severe conditions, especially temperature, could be examined to find more XOS in the produced liquor as well as affect cellulose in the lesser extent. This could be beneficial because of the energetic costs of high temperature as well as more favorable fractionation towards more valuable products such as XOS as well as glucose and lignin valorization products.
2) Higher pressure of CO_2 and higher solid to liquid ratio accompanied by lower temperature process could be study to examine the effect of CO_2 on the kinetics of the reaction as well as to optimize the reaction conditions in the respect of the obtained products [61].
3) The processed solid could be further valorized, using green catalysts such as enzymes to produce glucose. Glucose can be directly converted to ethanol or more valuable products can be obtained by chemical or biological valorization to levulinic acid and/or γ-valerolactone [89]. Furthermore untacked lignin can be valorized to accomplish the biorefinery concept idea.
4) The simple economic analysis (e.g. using green metrics approach [42, 90]) of the biorefinery concept developed on the proposed methods could be done to developed benchmark of the used processing techniques.

8. References

[1] H. Xie, N. Gathergood and J. Wiley, The Role of Green Chemistry in Biomass Processing and Conversion, Wiley Online Library, 2013.
[2] J.C. Escobar, E.S. Lora, O.J. Venturini, E.E. Yáñez, E.F. Castillo and O. Almazan, Renew. Sustain. Energ. Rev., 13 (2009) 1275.
[3] P.S. Nigam and A. Singh, Progr. Energy Combust. Sci., 37 (2011) 52.
[4] B. Kamm, P.R. Gruber and M. Kamm, Biorefineries–industrial processes and products, Wiley Online Library, 2007.
[5] E. Commission, Directive 2009/28/EC of the European Parliament and of the Council of 23 April 2009 on the promotion of the use of energy from renewable sources and amending and subsequently repealing Directives 2001/77/EC and 2003/30/EC, Official Journal of the European Union, Vol. L140, 2009, p. 16.
[6] S.P. Magalhães da Silva, A.M. da Costa Lopes, L.B. Roseiro and R. Bogel-Lukasik, RSC Adv., 3 (2013) 16040.
[7] D.R. Dodds and R.A. Gross, Science, 318 (2007) 1250.
[8] C.H. Christensen, J. Rass Hansen, C.C. Marsden, E. Taarning and K. Egeblad, ChemSusChem, 1 (2008) 283.
[9] L. Shen, J. Haufe and M.K. Patel, Report for European Polysaccharide Network of Excellence (EPNOE) and European Bioplastics, 243 (2009).
[10] J.E. Holladay, J.J. Bozell, J.F. White and D. Johnson, DOE Report PNNL-16983 (website: http://chembioprocess.pnl.gov/staff/staff_info.asp, acessed March 2014), (2007).
[11] SIADEB, www.siadeb.org, 2013, acessed March 2014.
[12] P.T. Anastas and J.C. Warner, Green Chemistry: Theory and Practice, Oxford University Press, New York, 1998.
[13] K. Soyez, B. Kamm and M. Kamm, The green biorefinery, Proceedings of 1st International Green Biorefinery Conference, Neuruppin, Germany 1997.
[14] A.R.C. Morais and R. Bogel-Lukasik, Sustain. Chem. Proces., 1:18 (2013).
[15] F. Cherubini, Energ. Convers. Manage., 51 (2010) 1412.
[16] E. de Jong, IEA Bioenergy, Task 42 Biorefinery, (2012).
[17] R.D. Perlack, L.L. Wright, A.F. Turhollow, R.L. Graham, B.J. Stokes and D.C. Erbach, Biomass as feedstock for a bioenergy and bioproducts industry: the technical feasibility of a billion-ton annual supply, DTIC Document, 2005.
[18] R. Sims, M. Taylor, J. Saddler and W. Mabee, International Energy Agency, (2008) 16.
[19] M. Galbe and G. Zacchi, Appl. Microbiol. Biotechnol., 59 (2002) 618.
[20] G.W. Huber, S. Iborra and A. Corma, Chem. Rev., 106 (2006) 4044.
[21] D.M. Alonso, S.G. Wettstein and J.A. Dumesic, Chem. Soc. Rev., 41 (2012) 8075.
[22] E.P.S. Bon and M.A. Ferrara, Bioethanol Production via Enzymatic Hydrolysis of Cellulosic Biomass, in FAO (Editor), The Role of Agricultural Biotechnologies for Production of Bioenergy in Developing Countries. FAO., Vol. 12, 2007.
[23] K. Ratanakhanokchai, R. Waeonukul, P. Pason, C. Tachaapaikoon, K.L. Kyu, K. Sakka, A. Kosugi and Y. Mori, in M.D. Matovic (Editor), Paenibacillus curdlanolyticus Strain

B-6 Multienzyme Complex: A Novel System for Biomass Utilization in Biomass Now - Cultivation and Utilization, INTECH, 2013.
[24] S. Kim and B.E. Dale, Biomass and bioenergy, 26 (2004) 361.
[25] J. Conti, Annual Energy Outlook 2007, Energy Information Administration (EIA) Energy Outlook, Modeling, and Data Conference, Washington, DC 2007.
[26] M.E. Zakrzewska, E. Bogel-Lukasik and R. Bogel-Lukasik, Chem. Rev., 111 (2011) 397.
[27] I.F.C. B.V, Applications of Furfural http://www.furan.com/furfural_applications_of_furfural.html, acessed May 2014
[28] A.F.A. Carvalho, P.D. Neto, D.F. Da Silva and G.M. Pastore, Food Research International, 51 (2013) 75.
[29] A. Samala, R. Srinivasan, M.P. Yadav, T.-J. Kim and L. Prewitt, Bioresources, 7 (2012).
[30] D. Stewart, Ind. Crop. Prod., 27 (2008) 202.
[31] W.O.S. Doherty, P. Mousavioun and C.M. Fellows, Ind. Crop. Prod., 33 (2011) 259.
[32] B. Kamm, M. Kamm, M. Schmidt, I. Starke and E. Kleinpeter, Chemosphere, 62 (2006) 97.
[33] M. FitzPatrick, P. Champagne, M.F. Cunningham and R.A. Whitney, Bioresour. Technol., 101 (2010) 8915.
[34] F. Carvalheiro, L.C. Duarte and F.M. Girio, J. Sci. Ind. Res., 67 (2008) 849.
[35] Y.-D. Tsai, Dilute Acid Hydrolysis of Oligomers in Hydrothermal Pretreatment Hydrolyzate into Monomers with High Yields, Vol. Master, University of California, 2012.
[36] V. Chaturvedi and P. Verma, 3 Biotech, 3 (2013) 415.
[37] M. Galbe and G. Zacchi, Biomass Bioenerg, 46 (2012) 70.
[38] S.P. Magalhães da Silva, A.R.C. Morais and R. Bogel-Lukasik, Green Chem., 16 (2014) 238.
[39] A.M. da Costa Lopes, K. João, A.R.C. Morais, E. Bogel-Lukasik and R. Bogel-Lukasik, Sustain. Chem. Proces., 1:3 (2013).
[40] A. Brandt, J. Gräsvik, J.P. Hallett and T. Welton, Green Chem., 15 (2013) 550.
[41] E.J. Beckman, J. Supercrit. Fluid., 28 (2004) 121.
[42] C.T. Matos, L. Gouveia, A.R.C. Morais, A. Reis and R. Bogel-Lukasik, Green Chem., 15 (2013) 2854.
[43] P.G. Jessop and W. Leitner, Chemical synthesis using supercritical fluids, John Wiley & Sons, 2008.
[44] L.C.S. Group, What are supercritical fluids?, http://www1.chem.leeds.ac.uk//People/CMR/whatarescf.html, acessed April 2014.
[45] R. Marriott and E. Sin, in H. Xie and N. Gathergood (Editors), Supercritical CO_2 as an Environmentally Benign Medium for Biorefinery in The Role of Green Chemistry in Biomass Processing and Conversion, John Wiley & Sons, Inc., 2013, p. 181.
[46] T.W. Randolph, H.W. Blanch and J.M. Prausnitz, AIChE J., 34 (1988) 1354.
[47] C.I. Melo, R. Bogel-Lukasik and E. Bogel-Lukasik, J. Supercrit. Fluid., 61 (2012) 191.
[48] G. Garrote, H. Dominguez and J.C. Parajo, Holz Als Roh-Und Werkstoff, 57 (1999) 191.
[49] N. Abatzoglou, E. Chornet, K. Belkacemi and R.P. Overend, Chem. Eng. Sci., 47 (1992) 1109.

[50] M. Rubio Torres, M. Heitz, G. Chauvette, E. Chornet and R.P. Overend, Biomass, 10 (1986) 85.
[51] J. Bouchard, T.S. Nguyen, E. Chornet and R.P. Overend, Biomass, 23 (1990) 243.
[52] F. Carvalheiro, L.C. Duarte and F.M. Gírio, Journal of Scientific & Industrial Research, 67 (2008) 849.
[53] F.M. Girio, C. Fonseca, F. Carvalheiro, L.C. Duarte, S. Marques and R. Bogel-Lukasik, Bioresour. Technol., 101 (2010) 4775.
[54] F. Carvalheiro, T. Silva-Fernandes, L.C. Duarte and F.M. Gírio, Appl. Biochem. Biotechnol., 153 (2009) 84.
[55] R.P. Overend, E. Chornet and J.A. Gascoigne, Philos.T. R. Soc. A, 321 (1987) 523.
[56] F. Carvalheiro, M.P. Esteves, J.C. Parajo, H. Pereira and F.M. Girio, Bioresour. Technol., 91 (2004) 93.
[57] M.E. Zakrzewska, E. Bogel-Łukasik and R. Bogel-Łukasik, Chemical reviews, 111 (2010) 397.
[58] G.P. van Walsum and H. Shi, Bioresour. Technol., 93 (2004) 217.
[59] Y. Kim, T. Kreke, N.S. Mosier and M.R. Ladisch, Biotechnol. Bioeng., 111 (2014) 254.
[60] N. Narayanaswamy, A. Faik, D.J. Goetz and T.Y. Gu, Bioresour. Technol., 102 (2011) 6995.
[61] A.R.C. Morais, A.C. Mata and R. Bogel-Lukasik, Green Chem., (2014) submitted.
[62] K.L. Toews, R.M. Shroll, C.M. Wai and N.G. Smart, Anal. Chem., 67 (1995) 4040.
[63] Z.H. Duan and R. Sun, Chem. Geol., 193 (2003) 257.
[64] A.J. Read, J. Solution Chem., 4 (1975) 53.
[65] G.P. van Walsum, Appl. Biochem. Biotechnol., 91-3 (2001) 317.
[66] H.L. Chum, D.K. Johnson, S.K. Black and R.P. Overend, Appl. Biochem. Biotechnol., 24-5 (1990) 1.
[67] B.L. Browning, in K.V. Sarkanen and C.H. Ludwig (Editors), Chemistry of Wood in Methods in Wood Chemistry, John Wiley & Sons, New York, 1967, p. 795.
[68] A.M. da Costa Lopes, K. João, D. Rubik, E. Bogel-Lukasik, L.C. Duarte, J. Andreaus and R. Bogel-Lukasik, Bioresour. Technol., 142 (2013) 198.
[69] D. Peng and D.B. Robinson, Industrial & Engineering Chemistry, 15 (1976) 59.
[70] O. Pfohl, S. Petkov and G. Brunner, PE V2.9.9a - Software for Phase Equilibria Calculations, Technische Universitat Hamburg-Harburg, Hamburg, Germany, 1998.
[71] F. Carvalheiro, G. Garrote, J.C. Parajo, H. Pereira and F.M. Girio, Biotechnol. Prog., 21 (2005) 233.
[72] G. Garrote, H. Dominguez and J.C. Parajo, Process Biochem. (Amsterdam, Neth.), 36 (2001) 571.
[73] B. Gullon, R. Yanez, J.L. Alonso and J.C. Parajo, Bioresour. Technol., 101 (2010) 6676.
[74] S. Ranganathan, D.G. Macdonald and N.N. Bakhshi, The Canadian Journal of Chemical Engineering, 63 (1985) 840.
[75] M.H. Sipponen, V. Pihlajaniemi, S. Sipponen, O. Pastinen and S. Laakso, RSC Adv., 4 (2014) 23177.
[76] M. Heitz, F. Carrasco, M. Rubio, G. Chauvette, E. Chornet, L. Jaulin and R.P. Overend, Can. J. Chem. Eng., 64 (1986) 647.

[77] G. Garrote and J.C. Parajo, Wood Sci. Technol., 36 (2002) 111.
[78] A. Garcia, M.G. Alriols, G. Spigno and J. Labidi, Biochemical Engineering Journal, 67 (2012) 173.
[79] D. Ciolacu, F. Ciolacu and V.I. Popa, Cellul. Chem. Technol., 45 (2011) 13.
[80] F.G. Hurtubise and H. Krässig, Anal. Chem., 32 (1960) 177.
[81] B.M. Kabyemela, M. Takigawa, T. Adschiri, R.M. Malaluan and K. Arai, Ind. Eng. Chem. Res., 37 (1998) 357.
[82] M. Sasaki, T. Adschiri and K. Arai, AIChE J., 50 (2004) 192.
[83] K.E. Vroom, Pulp & Paper Magazine Canada, 58 (1957) 228.
[84] T.A. Lloyd and C.E. Wyman, Bioresour. Technol., 96 (2005) 1967.
[85] G. Garrote, H. Dominguez and J.C. Parajo, J. Food Eng., 52 (2002) 211.
[86] R. Span and W. Wagner, J. Phys. Chem. Ref. Data, 25 (1996) 1509.
[87] A.S. Schmidt and A.B. Thomsen, Bioresour. Technol., 64 (1998) 139.
[88] E. Guerra-Rodriguez, O.M. Portilla-Rivera, L. Jarquin-Enriquez, J.A. Ramirez and M. Vazquez, Biomass Bioenerg, 36 (2012) 346.
[89] D.M. Alonso, S.G. Wettstein and J.A. Dumesic, Green Chem., 15 (2013) 584.
[90] R.A. Sheldon and J.P.M. Sanders, Catal. Today, (2014).

Appendix A. Example of the Calculations

A.1 – Liquor concentration

In the liquor phase sugar monomers, furfural and acetic and formic acid concentrations were calculated according to the signal area observed in HPLC spectrum using previously prepared calibration curves. The oligomer's determination was established by the difference between monomers' concentration after post-hydrolysis and monomers after pre-treatment.

Firstly, apart from oligomers, each compound concentration was calculated using the respective calibration curve. For each set of experiments a new calibration curve was prepared to avoid errors related to the HPLC column aging. For example to analyze glucose content in sample taken from experiment carried out for 30 minutes at 50 bar of initial CO_2 pressure the calibration curve with parameters as given in Equation A.1 were used.

$$Area_{Glc,Liquor} = 56594.38[Glc] - 2528.12 \qquad \text{Eq.A.1}$$

Analogous calibration curves and equations were established for each analyzed compound.

As it was discussed in the experimental section, the oligomer's concentration was obtained from the analysis of liquor subject to post-hydrolysis treatment. Therefore same calibration curve was used to calculate monomer's concentration in the post-hydrolysate. However, during the post-hydrolysis some sugars undergo degradation, thus, to calculate sugar oligomers, a correction factor F was introduced to correct these losses. According to Browning [67] the losses are 2.6% for glucose, 8.8% for xylose and 4.7% for arabinose .

$$[GOS]_{liquor} = \left([Glc]_{P.H} \times F \times \frac{\rho_{liquor}}{\rho_{H_2SO_4,4\%}} \times \frac{w_{sol,P.H}}{w_{liquor,P.H}} - [Glc]_{liquor}\right) \times \frac{M_{W,GOS}}{M_{W,Glc}} \qquad \text{Eq.A.2}$$

Where,

$$w_{sol,P.H} = w_{H_2SO_4,4\%} + w_{liquor,P.H} \qquad \text{Eq.A.3}$$

In the case of glucose

$$F = \frac{1}{1-0.026} = 1.027 \qquad \text{Eq.A.4}$$

The same algorithm was used for xylose, arabinose and their respective oligomers.

To model the behavior of the different compounds throughout the reaction, the percentage of each one in relation to the feedstock was calculated according to the Equation A.5 and A.6 for and sugar monomers/acetic acid and oligomers, respectively. The equations show the example of glucose and glucooligosaccharides as glucan feedstock (percentage by dry weight). In the case of furfural it was calculated as xylan and arabinoxylan feedstock, while HMF was assumed as glucan derivative. In turn, formic acid was considered the only degradation product from xylan/arainoxylan.

$$\%Glc\ as\ Gn_{feedstock} = \frac{m_{liquor} \times [Glc]_{liquor}}{\rho_{liquor} \times m_{feedstock} \times x_{Gn_{feedstock}}} \times \frac{M_{W,Gn}}{M_{w,Glc}} \times 100 \quad \text{Eq.A.5}$$

$$\%GOS\ as\ Gn_{feedstock} = \frac{x_{Glc_{liquor}} \times m_{dry\ liquor}}{m_{feedstock} \times x_{Gn_{feedstock}}} \times 100 - \%Glc\ as\ Gn_{feedstock} \quad \text{Eq.A.6}$$

Where:

$$x_{Glc_{liquor}} = F \times \frac{m_{sol,PH} \times [Glc]_{P.H}}{\rho_{H_2SO_4,4\%} \times m_{dry\ liquor,P.H}} \times \frac{M_{W,Gn}}{M_{w,Glc}} \quad \text{Eq.A.7}$$

A.2 – Treated solids composition

The same calculation for liquid was done to determine the remaining fraction of glucan, xylan, arabinan and acetyl groups in the solid residue according to the Equation A.8. Thus consecutively Equation A.9 can be proposed and is similar to A.7, but this time the results were obtained from quantitative acid hydrolysis of the processed solid.

$$\%Remaining\ Gn = \frac{m_{solid\ residue}}{m_{feedstock}} \times \frac{x_{Gn_{residue}}}{x_{feedstock}} \times 100 \quad \text{Eq.A.8}$$

where

$$x_{Gn_{residue}} = F \times \frac{m_{sol,QAC} \times [Glc]_{QAC}}{\rho_{H_2SO_4,4\%} \times m_{dry\ solid,QAC}} \times \frac{M_{W,Gn}}{M_{w,Glc}} \quad \text{Eq.A.9}$$

The results obtained from the Equations A.5 to A.9 were normalized considering a recuperation of 100%. Equation A.10 shows the example of normalized remaining glucan. The same calculation was done for all compounds in the liquor.

$$\%Gn_{normalized} = \frac{\%Gn \times 100}{\%Gn + \%GOS + \%Glc + \%HMF + \%DP} \quad \text{Eq.A.10}$$

Analogous procedure was applied for xylan, arabinoxylan and acetyl groups.